

Explaining the $b \rightarrow s\ell^+\ell^-$ anomalies in Z' scenarios with top-FCNC couplings

Xin-Qiang Li^{1,*}, Meng Shen^{1,†}, Dong-Yang Wang^{2,‡},
Ya-Dong Yang^{1,3,§}, and Xing-Bo Yuan^{1,¶}

¹ Institute of Particle Physics and Key Laboratory of Quark and Lepton Physics (MOE),
Central China Normal University, Wuhan, Hubei 430079, China

² Department of Physics, Jiujiang University, Jiujiang 332005, China

³ School of Physics and Microelectronics, Zhengzhou University, Zhengzhou, Henan 450001, China

Abstract

Motivated by the recent anomalies in $b \rightarrow s\ell^+\ell^-$ transitions, we explore a minimal Z' scenario, in which the Z' boson has a flavour-changing coupling to charm and top quarks and a flavour-conserving coupling to muons. It is found that such a Z' boson can explain the current $b \rightarrow s\ell^+\ell^-$ anomalies, while satisfying other flavour and collider constraints simultaneously. The Z' boson can be as light as few hundreds GeV. In this case, the $t \rightarrow c\mu^+\mu^-$ decay and the tZ' associated production at the LHC could provide sensitive probes of such a Z' boson. As a special feature, the Z' contributions to all rare B - and K -meson processes are controlled by one parameter. This results in interesting correlations among these processes, which could provide further insights into this scenario. In addition, an extended scenario, in which the Z' boson interacts with the $SU(2)_L$ fermion doublets with analogous couplings as in the minimal scenario, is also investigated.

*xqli@ccnu.edu.cn

†shenmeng@mails.ccnu.edu.cn

‡wangdongyang@mails.ccnu.edu.cn

§yangyd@ccnu.edu.cn

¶y@ccnu.edu.cn

1 Introduction

The flavour-changing neutral current (FCNC) processes are sensitive to possible contributions from heavy mediators and provide a complementary way to direct searches for new physics (NP) at high-energy frontiers. While there is so far no direct evidence for NP at the LHC, recent measurements of the rare $b \rightarrow s\ell^+\ell^-$ decays exhibit several interesting discrepancies from the Standard Model (SM) predictions of the branching ratios, the angular distributions, and the lepton flavour universality (LFU) ratios [1–4].

In this respect, the ratios defined as $R_{K^{(*)}} \equiv \mathcal{B}(B \rightarrow K^{(*)}\mu^+\mu^-)/\mathcal{B}(B \rightarrow K^{(*)}e^+e^-)$ are of particular interest, because the hadronic uncertainties largely cancel out here [5]. Therefore, they provide a sensitive test of the LFU. In the SM, these ratios are predicted to be close to unity up to tiny electromagnetic corrections [5–8]. Recently, the LHCb collaboration presented an updated measurement of R_K using the full data set of 9 fb^{-1} [9]:

$$R_K = 0.846_{-0.039}^{+0.042}(\text{stat})_{-0.012}^{+0.013}(\text{syst}), \quad \text{for } 1.1 < q^2 < 6.0 \text{ GeV}^2, \quad (1)$$

where q^2 denotes the dilepton invariant mass squared. This new result confirms the previous LHCb measurement using a data set of 5 fb^{-1} [10]. However, the tension with the SM prediction has increased from previously 2.5σ to now 3.1σ , due to reduced experimental uncertainties. LHCb has also reported a measurement of R_{K^*} using the full Run-I data set of 3 fb^{-1} [11]:

$$R_{K^*} = \begin{cases} 0.66_{-0.07}^{+0.11}(\text{stat}) \pm 0.03(\text{syst}), & 0.045 < q^2 < 1.1 \text{ GeV}^2, \\ 0.69_{-0.07}^{+0.11}(\text{stat}) \pm 0.05(\text{syst}), & 1.1 < q^2 < 6.0 \text{ GeV}^2, \end{cases} \quad (2)$$

which are found to be about 2.1σ and 2.4σ lower than the SM predictions, respectively. Very recently, the LHCb measurements of R_{K_S} and $R_{K^{*+}}$ have also been reported [12]. Previous measurements from the BaBar [13] and Belle [14, 15] experiments are also consistent with the LHCb results, although with relatively large uncertainties. All these measurements of R_K and R_{K^*} together provide intriguing hints of the LFU violation.

Recently, the LHCb collaboration reported the most precise measurement of the branching ratio of the $B_s \rightarrow \phi\mu^+\mu^-$ decay using the full Run-1 and Run-2 data sets [16],

$$\mathcal{B}(B_s \rightarrow \phi\mu^+\mu^-) = (2.88 \pm 0.15 \pm 0.05 \pm 0.14) \times 10^{-8}, \quad \text{for } 1.1 < q^2 < 6.0 \text{ GeV}^2, \quad (3)$$

where the uncertainties are, in order, statistical, systematic, and from the branching fraction of the normalization mode. This measurement is found to lie 3.6σ below the SM prediction [17–20]. Using the same full data set, LHCb later presented an improved measurement of the branching ratio of the rare $B_s \rightarrow \mu^+\mu^-$ decay [21],

$$\mathcal{B}(B_s \rightarrow \mu^+\mu^-) = [3.09_{-0.43}^{+0.46}(\text{stat})_{-0.11}^{+0.15}(\text{syst})] \times 10^{-9}, \quad (4)$$

which is statistically consistent with the previous world average [22]. This new result is compatible with the SM expectation [23, 24] within 1σ . However, after combining all the measurements of the $B_{s,d} \rightarrow \mu^+\mu^-$ decays from the ATLAS [25], CMS [26], and LHCb [21] experiments, the total discrepancy with the SM is found to be at the level of 2σ [27, 28]. In addition, the latest measurements of the $B^0 \rightarrow K^{*0}\mu^+\mu^-$ [29] and $B^+ \rightarrow K^{*+}\mu^+\mu^-$ [30] decays show tensions in the angular distributions with respect to the SM predictions. The local discrepancies in the angular observables P_2 and P'_5 are observed to be at $2.5\text{--}3.0\sigma$ in two q^2 bins [29, 30].

Although none of the individual deviations is statistically significant, and further refinement of the hadronic uncertainties in some observables is still an ongoing theoretical issue [31–33], the global tension in the $b \rightarrow s\ell^+\ell^-$ decays has motivated a lot of NP interpretations [1–4]. In this respect, one of the most popular NP explanations are models with an extra heavy vector Z' boson. In these models, the Z' boson has couplings to quarks, as well as to either electrons or muons. Depending on the quark couplings involved, these Z' models can be classified into two categories: (i) The Z' boson has flavour-violating couplings to b and s quarks and the $b \rightarrow s\ell^+\ell^-$ transitions receive contributions from tree-level Z' exchange [34–58]. (ii) The Z' boson has flavour-conserving couplings to top quark and affects the $b \rightarrow s\ell^+\ell^-$ transitions via one-loop penguin diagrams [59, 60]. In this paper, based on our previous works [61, 62], we will consider another possibility, where the Z' boson has flavour-violating couplings to top and charm quarks. This scenario does not suffer from the constraints from $B_s - \bar{B}_s$ mixing, and the Z' boson contributes to the $b \rightarrow s\ell^+\ell^-$ decays at the one-loop level. We will derive constraints on the Z' mass and couplings from various flavour and collider processes, and study the possibility of explaining the $b \rightarrow s\ell^+\ell^-$ anomalies in such a scenario. Future prospects of searching for such a Z' boson at the LHC will also be discussed.

This paper is organized as follows. In section 2, we introduce the phenomenological Z'

scenarios, which have the desired flavour-changing couplings to explain the current $b \rightarrow s\ell^+\ell^-$ anomalies. In section 3, we recapitulate the theoretical frameworks for various flavour processes and discuss the Z' effects. In section 4, we give our detailed numerical results and discussions. Our conclusions are finally made in section 5.

2 Z' scenarios with top-quark FCNC couplings

We consider two phenomenological scenarios involving a Z' boson. In the first scenario (denoted as scenario I), the Z' boson has flavour-changing couplings to c and t quarks and a flavour-conserving coupling to the μ lepton. Their interactions are described by the effective Lagrangian

$$\mathcal{L}_{Z'}^{\text{I}} = (X_{ct}^L \bar{c}\gamma^\mu P_L t Z'_\mu + \text{h.c.}) + \lambda_{\mu\mu}^L \bar{\mu}\gamma^\mu P_L \mu Z'_\mu, \quad (5)$$

where $P_L = (1 - \gamma_5)/2$, and the fermion fields c , t and μ refer to the mass eigenstates. Generally, the couplings X_{ct}^L and $\lambda_{\mu\mu}^L$ are complex and real, respectively. In this scenario, the Z' boson affects the $b \rightarrow s\mu^+\mu^-$ transitions via one-loop penguin diagram and could explain the anomalies observed in $B \rightarrow K^{(*)}\ell^+\ell^-$ decays. Furthermore, sizable contributions to the $s \rightarrow d\mu^+\mu^-$ transitions could arise from the Z' penguin diagram.

In the second scenario (denoted as scenario II), the Z' boson is assumed to interact with the $SU(2)_L$ fermion doublets with similar couplings as in scenario I. In the mass eigenstate basis, the effective Lagrangian takes the form¹

$$\begin{aligned} \mathcal{L}_{Z'}^{\text{II}} &= (X_{23}^L \bar{Q}_{L,2}\gamma^\mu Q_{L,3} Z'_\mu + \text{h.c.}) + \lambda_{22}^L \bar{L}_{L,2}\gamma^\mu L_{L,2} Z'_\mu \\ &= [X_{23}^L (\bar{c}\gamma^\mu P_L t + \bar{s}\gamma^\mu P_L b) Z'_\mu + \text{h.c.}] + \lambda_{22}^L (\bar{\mu}\gamma^\mu P_L \mu + \bar{\nu}_\mu\gamma^\mu P_L \nu_\mu) Z'_\mu, \end{aligned} \quad (6)$$

where $Q_{L,i}$ and $L_{L,i}$ denote the left-handed $SU(2)_L$ quark and lepton doublets of the i -th generation, respectively. As in scenario I, the couplings X_{23}^L and λ_{22}^L are generally complex and real, respectively. In this scenario, the $b\bar{s}Z'$ and the $t\bar{c}Z'$ interaction have the same coupling strength due to $SU(2)_L$ invariance. As a consequence, the Z' contribution to $b \rightarrow s$ processes is mainly induced by the $b\bar{s}Z'$ interaction at the tree level, and the phenomenology of these processes is similar to that in the so-called minimal Z' scenario discussed in refs. [34, 45]. As

¹In ref. [63], a similar Z' scenario has been discussed, where the Z' boson has left-handed couplings to the lepton doublets but only right-handed couplings to the up-type quarks.

in scenario I but contrary to the minimal Z' scenario, the $s \rightarrow d$ transitions can receive the Z' contribution at the one-loop level. Furthermore, the Z' boson also couples to the muon neutrino due to $SU(2)_L$ invariance, which may affect the $b \rightarrow s\nu\bar{\nu}$ and $s \rightarrow d\nu\bar{\nu}$ processes. The Z' effects in various flavour processes will be discussed in detail in the next section.

Alternatively, one can consider a Z' boson with flavour-changing couplings to u and t instead of c and t quarks in the above scenarios. Then, the Z' contributions to the top-quark production and FCNC decays can be very different from that in scenarios I and II. For the Z' couplings to leptons, a right-handed $\mu^+\mu^-Z'$ interaction can also be added to simultaneously accommodate the $b \rightarrow s\mu^+\mu^-$ and $(g-2)_\mu$ anomalies [64, 65]. Similarly, scenarios with an e^+e^-Z' instead of a $\mu^+\mu^-Z'$ coupling in the above scenarios can also be considered. Such a Z' boson could be directly produced in e^+e^- colliders, but loses the possibility of explaining the $(g-2)_\mu$ anomaly. We leave all these possibilities for future studies, and consider in this paper only the above two scenarios that have the couplings required to explain the $b \rightarrow s\ell^+\ell^-$ anomalies.

3 Z' effects in various flavour processes

In this section, we recapitulate the theoretical frameworks for various low-energy flavour processes and discuss the Z' contributions to them as well as to the top-quark physics.

3.1 $b \rightarrow s\mu^+\mu^-$ transitions

The rare decays $B_s \rightarrow \mu^+\mu^-$, $B \rightarrow K^{(*)}\mu^+\mu^-$, and $B_s \rightarrow \phi\mu^+\mu^-$ are induced by the $b \rightarrow s\mu^+\mu^-$ transitions, and provide promising probes of NP effects. With the Z' contributions taken into account, the effective Hamiltonian for the $b \rightarrow s\mu^+\mu^-$ transitions can be written as [66]

$$\mathcal{H}_{\text{eff}}^{b \rightarrow s\mu^+\mu^-} = -\frac{4G_F}{\sqrt{2}}V_{tb}V_{ts}^* \sum_{i=1}^{10} C_i \mathcal{O}_i, \quad (7)$$

where explicit definitions of the effective operators \mathcal{O}_{1-8} can be found in ref. [66]. The operators most relevant to our study are, however, the two semi-leptonic operators $\mathcal{O}_{9\ell}$ and $\mathcal{O}_{10\ell}$ defined by

$$\mathcal{O}_{9\ell} = \frac{e^2}{16\pi^2}(\bar{s}\gamma_\mu P_L b)(\bar{\ell}\gamma^\mu \ell), \quad \text{and} \quad \mathcal{O}_{10\ell} = \frac{e^2}{16\pi^2}(\bar{s}\gamma_\mu P_L b)(\bar{\ell}\gamma^\mu \gamma_5 \ell), \quad (8)$$

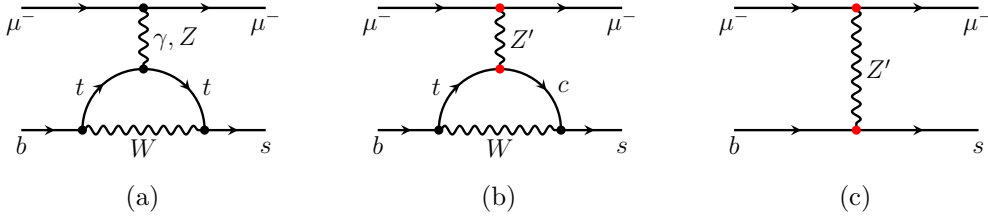


Figure 1: Feynman diagrams for the $b \rightarrow s\mu^+\mu^-$ transitions, including the selected SM penguin contributions (a), as well as the Z' effects from the scenarios I (b) and II (b, c).

respectively. In the SM, their Wilson coefficients have been calculated including next-to-next-to-leading-order (NNLO) QCD [67–69] and next-to-leading-order (NLO) electroweak corrections [70]. In the Z' scenario I, the $t\bar{c}Z'$ vertex can affect the $b \rightarrow s\mu^+\mu^-$ transitions through the Z' -penguin diagram shown in figure 1 (b), with the resulting NP Wilson coefficients given by [61, 62]

$$\mathcal{C}_{9\mu}^{\text{NP,I}} = -\mathcal{C}_{10\mu}^{\text{NP,I}} = \frac{1}{8\sqrt{2}G_F s_W^2} \frac{V_{cs}^*}{V_{ts}^*} \frac{X_{ct}^L \lambda_{\mu\mu}^L}{m_{Z'}^2} f(x_t), \quad (9)$$

with $s_W = \sin\theta_W$, $x_t = \bar{m}_t(\bar{m}_t)^2/m_W^2$, and V_{ij} the Cabibbo-Kobayashi-Maskawa (CKM) matrix elements [71, 72]. The loop function $f(x)$ is defined as

$$f(x) = \frac{3}{2} + x \log \frac{\mu^2}{m_W^2} + x - x \log x, \quad (10)$$

which is obtained from the calculation of similar diagrams with anomalous $t\bar{c}Z$ vertex in refs. [61, 62]. It is noted that the Z' contributions are enhanced by the CKM factor V_{cs}/V_{ts} . In the Z' scenario II, the Z' boson can also affect the $b \rightarrow s\mu^+\mu^-$ transitions at tree level through the diagram in figure 1 (c). The total contributions to the NP Wilson coefficients are given by

$$\mathcal{C}_{9\mu}^{\text{NP,II}} = -\mathcal{C}_{10\mu}^{\text{NP,II}} = \frac{1}{\sqrt{2}G_F} \left(\frac{1}{8s_W^2} \frac{V_{cs}^*}{V_{ts}^*} f(x_t) - \frac{\pi}{\alpha_e V_{tb} V_{ts}^*} \right) \frac{X_{23}^L \lambda_{22}^L}{m_{Z'}^2}. \quad (11)$$

Numerically, it is found that the tree-level contribution is dominant and the loop-level contribution can be safely neglected. For $m_{Z'} = 1$ TeV, $\mathcal{C}_{9\mu}^{\text{NP,I}} = (-4.4 - 0.1i)X_{ct}^L \lambda_{\mu\mu}^L$ in scenario I, while $\mathcal{C}_{9\mu}^{\text{NP,II}} = (585 + 11i)X_{23}^L \lambda_{22}^L$ in scenario II.

A lot of effort has been put into the theoretical treatment of $B \rightarrow K\mu^+\mu^-$, $B \rightarrow K^*\mu^+\mu^-$, and $B_s \rightarrow \phi\mu^+\mu^-$ decays [19, 33, 73–77]. Besides the LFU ratios $R_{K^{(*)}}$ introduced in section 1, the angular observables in these decays are also known to provide valuable information of potential NP contributions, and hence have been analyzed in detail in refs. [78, 79]. For these

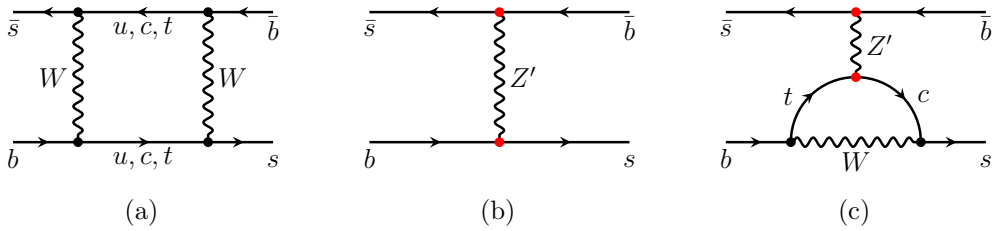


Figure 2: Feynman diagrams for the $B_s - \bar{B}_s$ mixing both within the SM (a) and in the Z' scenario II (b, c). For each diagram, there is also a second one obtained by a 90° rotation.

observables, the main theoretical uncertainties come from the heavy-to-light transition form factors. During recent years, significant progress has been made in calculating these form factors from lattice QCD [18, 80] and light-cone sum rules (LCSR) [19, 81–85]. For a recent review of the $b \rightarrow s\mu^+\mu^-$ decays, we refer to refs. [86–88], where the SM calculations, input parameters, form factors, and theoretical uncertainties are discussed in detail.

3.2 $B_s - \bar{B}_s$ mixing

The $B_s - \bar{B}_s$ mixing is induced by the W -box diagram in the SM, and could receive contributions from the tree and penguin diagrams in the Z' scenario II, as shown in figure 2. The effective Hamiltonian for $B_s - \bar{B}_s$ mixing can be written as [89]

$$\mathcal{H}_{\text{eff}}^{\Delta B=2} = \frac{G_F^2}{16\pi^2} m_W^2 (V_{tb}V_{ts}^*)^2 \mathcal{C}^{\text{VLL}} \mathcal{O}^{\text{VLL}} + \text{h.c.}, \quad (12)$$

with the effective operator $\mathcal{O}^{\text{VLL}} = (\bar{s}\gamma_\mu P_L b)(\bar{s}\gamma^\mu P_L b)$. Analytical expression of the SM Wilson coefficient $\mathcal{C}_{\text{SM}}^{\text{VLL}}$ and the QCD renormalization group evolution (RGE) can be found in refs. [66, 90] and [89, 91], respectively. In the Z' scenario II, the Z' -penguin diagram shown in figure 2 (c) is found to be negligible, and the tree-level Z' -exchange diagram shown in figure 2 (b) results in the NP contribution

$$\mathcal{C}_{\text{NP,II}}^{\text{VLL}} = \frac{8\pi^2}{G_F^2 m_W^2} \frac{1}{(V_{tb}V_{ts}^*)^2} \left(\frac{X_{23}^L}{m_{Z'}} \right)^2. \quad (13)$$

In the Z' scenario I, the Z' boson contributes to the $B_s - \bar{B}_s$ mixing starting at the two-loop level, and its effects are therefore expected to be small. Here we will take $\mathcal{C}_{\text{NP,I}}^{\text{VLL}} = 0$.

With the effective Hamiltonian in eq. (12), the off-diagonal mass matrix element of $B_s - \bar{B}_s$

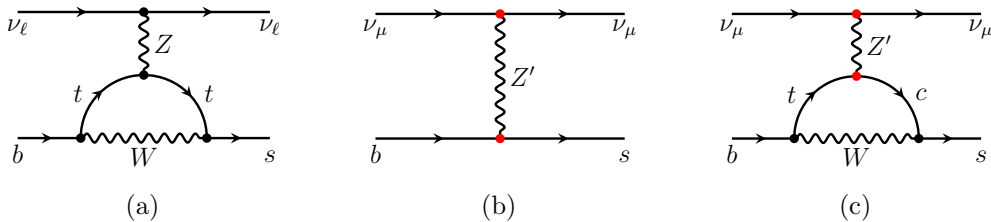


Figure 3: Feynman diagrams for the $b \rightarrow s\nu\bar{\nu}$ transition, including the selected SM diagram (a), and the Z' contributions in the scenario II (b, c).

mixing is given by [89]

$$M_{12}^s = \langle B_s | \mathcal{H}_{\text{eff}}^{\Delta B=2} | \bar{B}_s \rangle = \frac{G_F^2}{16\pi^2} m_W^2 (V_{tb}V_{ts}^*)^2 \mathcal{C}^{\text{VLL}} \langle B_s | \mathcal{O}^{\text{VLL}} | \bar{B}_s \rangle, \quad (14)$$

where $\mathcal{C}^{\text{VLL}} = \mathcal{C}_{\text{SM}}^{\text{VLL}} + \mathcal{C}_{\text{NP}}^{\text{VLL}}$, and the most recent lattice calculations of the hadronic matrix element $\langle B_s | \mathcal{O}^{\text{VLL}} | \bar{B}_s \rangle$ can be found in ref. [80]. Then, the mass difference between the two mass eigenstates B_s^H and B_s^L and the CP violation phase read [92]

$$\Delta m_s = 2|M_{12}^s|, \quad \text{and} \quad \phi_s = \arg M_{12}^s, \quad (15)$$

respectively. In the case with a complex Z' coupling X_{23}^L , the phase ϕ_s can deviate from the SM prediction and hence affects the CP violation $S_{\psi\phi}$ measured in the decay $B_s \rightarrow J/\psi\phi$ [92].

3.3 $b \rightarrow s\nu\bar{\nu}$ decays

The rare decays $B \rightarrow X_s\nu\bar{\nu}$ and $B \rightarrow K^{(*)}\nu\bar{\nu}$ are all induced by the quark-level $b \rightarrow s\nu\bar{\nu}$ transition. With the Z' effects taken into account, the effective Hamiltonian governing the $b \rightarrow s\nu\bar{\nu}$ decays can be written as [93, 94]

$$\mathcal{H}_{\text{eff}}^{b \rightarrow s\nu\bar{\nu}} = \frac{4G_F}{\sqrt{2}} \frac{\alpha_e}{2\pi s_W^2} V_{tb}V_{ts}^* \sum_{\ell=e,\mu,\tau} \mathcal{C}_\ell(\bar{s}\gamma_\mu P_L b) (\bar{\nu}_\ell\gamma^\mu P_L \nu_\ell) + \text{h.c.}, \quad (16)$$

where ℓ denotes the neutrino flavour. In the SM, the Wilson coefficient $\mathcal{C}_\ell^{\text{SM}}(\mu_W) = X(x_t)$ are induced by the Z -penguin and W -box diagrams, and are lepton flavour universal. Analytical expression of the Inami-Lim function $X(x_t)$ can be found in refs. [95, 96]. Numerically, we obtain $\mathcal{C}_\ell^{\text{SM}}(\mu_W) = 1.481 \pm 0.009$ [97] after including the two-loop electroweak corrections [98]. In the Z' scenario II, the tree-level and the one-loop penguin diagram shown in figure 3 contribute to

the $b \rightarrow s\nu_\mu\bar{\nu}_\mu$ transition, resulting in

$$\mathcal{C}_\mu^{\text{NP},\text{II}}(\mu_W) = -\frac{1}{\sqrt{2}G_F} \left(\frac{1}{8} \frac{V_{cs}^*}{V_{ts}^*} f(x_t) - \frac{\pi s_W^2}{\alpha_e V_{tb} V_{ts}^*} \right) \frac{X_{23}^L \lambda_{22}^L}{m_{Z'}^2}, \quad (17)$$

with the loop function $f(x_t)$ defined already by eq. (10). Numerically, the tree-level Z' -exchange contribution dominates over that from the one-loop Z' -penguin diagram, as in $b \rightarrow s\mu^+\mu^-$ decays. As there are no couplings of the Z' boson to ν_e and ν_τ neutrinos, $\mathcal{C}_e^{\text{NP},\text{II}} = \mathcal{C}_\tau^{\text{NP},\text{II}} = 0$. In the Z' scenario I, there is no direct coupling of the Z' boson to neutrinos. The Z' boson contributes to the $b \rightarrow s\nu\bar{\nu}$ transition at least at the two-loop level and hence can be safely neglected, i.e. $\mathcal{C}_\ell^{\text{NP},\text{I}} = 0$.

The inclusive decay $B \rightarrow X_s\nu\bar{\nu}$ is the theoretically cleanest rare B -meson decay [99]. With the effective Hamiltonian in eq. (16), its differential decay width can be written as [93]

$$\frac{d\Gamma(B \rightarrow X_s\nu\bar{\nu})}{ds_b} = N(m_b, m_s) \kappa(0) [3s_b (1 + \hat{m}_s^2 - s_b) + \lambda(1, \hat{m}_s^2, s_b)] \sum_{\ell=e,\mu,\tau} |\mathcal{C}_\ell(\mu_W)|^2, \quad (18)$$

with the overall factor given by

$$N(m_1, m_2) = \frac{G_F^2 \alpha_e^2 m_1^5}{384\pi^5 s_W^4} |V_{tb} V_{ts}^*|^2 \lambda^{1/2} \left(1, \frac{m_2^2}{m_1^2}, \frac{q^2}{m_1^2} \right), \quad (19)$$

where $\lambda(x, y, z) = x^2 + y^2 + z^2 - 2(xy + yz + zx)$, $\hat{m}_i = m_i/m_b$, and $s_b = q^2/m_b^2$ with q^2 the invariant mass squared of the neutrino pair. The factor $\kappa(0) = 0.83$ contains the virtual and bremsstrahlung QCD corrections to the $b \rightarrow s\nu\bar{\nu}$ matrix element [100, 101].

For the exclusive decay $B \rightarrow K\nu\bar{\nu}$, the dineutrino invariant mass distribution reads [93, 102]

$$\frac{d\Gamma(B \rightarrow K\nu\bar{\nu})}{ds_B} = \frac{1}{2} N(m_B, m_K) \lambda(1, \tilde{m}_K^2, s_B) [f_+^{B \rightarrow K}(s_B)]^2 \sum_{\ell=e,\mu,\tau} |\mathcal{C}_\ell(\mu_W)|^2, \quad (20)$$

where $\tilde{m}_K = m_K/m_B$, $s_B = q^2/m_B^2$, and q^2 denotes the dineutrino invariant mass squared. The $B \rightarrow K$ form factor $f_+^{B \rightarrow K}(s_B)$ is the main source of theoretical uncertainties. Recent lattice QCD and LCSR results for $f_+^{B \rightarrow K}(s_B)$ can be found in refs. [103, 104] and [82, 105], respectively.

For the $B \rightarrow K^*\nu\bar{\nu}$ decay, the dineutrino invariant mass spectrum can be written as [93]

$$\frac{d\Gamma(B \rightarrow K^*\nu\bar{\nu})}{ds_B} = \frac{1}{8} N(m_B, m_{K^*}) s_B \sum_{\ell=e,\mu,\tau} \left(|A_\perp^\ell(s_B)|^2 + |A_\parallel^\ell(s_B)|^2 + |A_0^\ell(s_B)|^2 \right), \quad (21)$$

with the three transversity amplitudes given, respectively, as

$$A_\perp(s_B) = -2\sqrt{2} \lambda^{1/2}(1, \tilde{m}_{K^*}^2, s_B) \mathcal{C}_\ell(\mu_W) \frac{V(s_B)}{1 + \tilde{m}_{K^*}^2}, \quad (22)$$

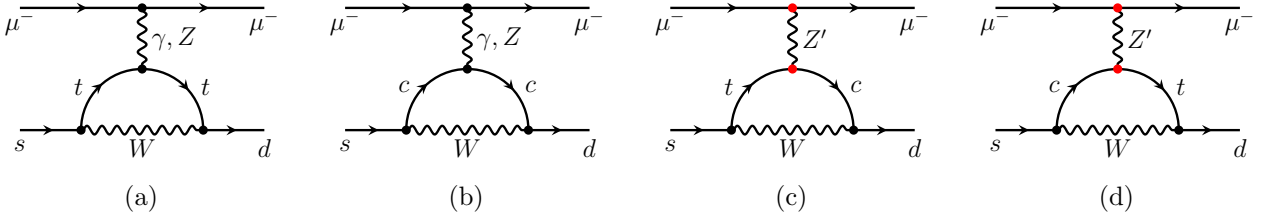


Figure 4: Feynman diagrams for the $s \rightarrow d\mu^+\mu^-$ transition, including the selected SM diagrams (a, b), and the Z' contributions (c, d).

$$A_{\parallel}(s_B) = 2\sqrt{2}(1 + \tilde{m}_{K^*})\mathcal{C}_\ell(\mu_W)A_1(s_B),$$

$$A_0(s_B) = \frac{\mathcal{C}_\ell(\mu_W)}{\tilde{m}_{K^*}\sqrt{s_B}} \left[(1 - \tilde{m}_{K^*}^2 - s_B)(1 + \tilde{m}_{K^*})A_1(s_B) - \lambda(1, \tilde{m}_{K^*}^2, s_B) \frac{A_2(s_B)}{1 + \tilde{m}_{K^*}} \right],$$

where $\tilde{m}_{K^*} = m_{K^*}/m_B$. Here, the main theoretical uncertainties arise from the three $B \rightarrow K^*$ transition form factors $V(s_B)$, $A_1(s_B)$ and $A_2(s_B)$. Recent lattice QCD and LCSR calculations of these form factors can be found in refs. [80, 106] and refs. [19, 82, 84], respectively.

3.4 $s \rightarrow d\mu^+\mu^-$ transition

For the $s \rightarrow d\mu^+\mu^-$ transition, the most relevant decay modes are the $K_{L,S} \rightarrow \mu^+\mu^-$ decays. After taking into account the Z' effects, the effective Hamiltonian inducing the short-distance (SD) contribution to $K_{L,S} \rightarrow \mu^+\mu^-$ decays can be written as [107]

$$\mathcal{H}_{\text{eff}}^{s \rightarrow d\mu^+\mu^-} = \frac{4G_F}{\sqrt{2}} \frac{\alpha_e}{4\pi s_W^2} (V_{ts}^* V_{td} Y + V_{cs}^* V_{cd} Y_{\text{NL}}) (\bar{s}\gamma_\mu P_L d) (\bar{\mu}\gamma^\mu \gamma_5 \mu) + \text{h.c.} \quad (23)$$

In the SM, the function $Y = Y(x_t)$ describes contributions from the penguin diagrams with internal top quark [69, 70, 95, 96], while Y_{NL} involves the charm-quark contributions [108]. In both the Z' scenarios I and II, the $s \rightarrow d\mu^+\mu^-$ transition is induced by the penguin diagrams shown in figure 4, which result in the NP contributions

$$Y_{\text{NP,I}} = \frac{1}{8\sqrt{2}G_F} \left(\frac{V_{cd}}{V_{td}} \frac{X_{ct}^{L*} \lambda_{\mu\mu}^L}{m_{Z'}^2} + \frac{V_{cs}^*}{V_{ts}^*} \frac{X_{ct}^L \lambda_{\mu\mu}^L}{m_{Z'}^2} \right) f(x_t), \quad (24)$$

$$Y_{\text{NP,II}} = \frac{1}{8\sqrt{2}G_F} \left(\frac{V_{cd}}{V_{td}} \frac{X_{23}^{L*} \lambda_{22}^L}{m_{Z'}^2} + \frac{V_{cs}^*}{V_{ts}^*} \frac{X_{23}^L \lambda_{22}^L}{m_{Z'}^2} \right) f(x_t), \quad (25)$$

with the loop function $f(x_t)$ defined already in eq. (10). Here, the NP contributions in both of the two Z' scenarios are of the same magnitude, which is different from what is observed in the $b \rightarrow s\mu^+\mu^-$ transitions. Numerically, $Y = 0.94 - (1.03 + 0.02i)X_{ct}^L \lambda_{\mu\mu}^L - (0.99 + 0.45i)X_{ct}^{L*} \lambda_{\mu\mu}^L$

for $m_{Z'} = 1 \text{ TeV}$ in scenario I.

For the $K_{L,S} \rightarrow \mu^+ \mu^-$ decays, only the SD part of a dispersive contribution can be reliably calculated. The branching ratio of $K_L \rightarrow \mu^+ \mu^-$ can be written as [107]

$$\mathcal{B}(K_L \rightarrow \mu^+ \mu^-)_{\text{SD}} = \kappa_\mu \left[\frac{\text{Re}(\lambda_t Y)}{\lambda^5} + \frac{\text{Re}\lambda_c}{\lambda} P_c(Y) \right]^2, \quad (26)$$

with $\lambda_t = V_{ts}^* V_{td}$, $\lambda_c = V_{cs}^* V_{cd}$, and $\lambda \approx V_{us}$ denoting the Wolfenstein parameter. The factor κ_μ contains the relevant hadronic matrix element that can be extracted from the $K^+ \rightarrow \mu^+ \nu_\mu$ decay, and numerically we have $\kappa_\mu = (2.009 \pm 0.017) \times 10^{-9} (\lambda/0.225)^8$ [107, 108]. The charm contribution $P_c(Y)$ is found to be $P_c(Y) = 0.115 \pm 0.017$ at the NNLO in QCD [108]. For the $K_S \rightarrow \mu^+ \mu^-$ decay, the SD and long-distance contributions add incoherently in the total rate [109–112]. The SD part of the branching ratio is given by [109–112]

$$\mathcal{B}(K_S \rightarrow \mu^+ \mu^-)_{\text{SD}} = \tau_{K_S} \frac{G_F^2 \alpha_e^2}{8\pi^3 s_W^4} m_K f_K^2 \left(1 - \frac{m_\mu^2}{m_K^2} \right)^{1/2} m_\mu^2 \text{Im}^2(\lambda_t Y), \quad (27)$$

with τ_{K_S} the lifetime of K_S and f_K the decay constant.

3.5 $s \rightarrow d\nu\bar{\nu}$ decays

The $K^+ \rightarrow \pi^+ \nu\bar{\nu}$ and $K_L \rightarrow \pi^0 \nu\bar{\nu}$ decays are induced by the $s \rightarrow d\nu\bar{\nu}$ transition. They are both characterized by the theoretically clean virtue, since the relevant hadronic matrix elements can be extracted with the help of isospin symmetry from the leading semi-leptonic $K_{\ell 3}$ decays [113]. With the Z' effects taken into account, the $s \rightarrow d\nu\bar{\nu}$ decays are governed by the effective Hamiltonian [95, 96]

$$\mathcal{H}_{\text{eff}}^{s \rightarrow d\nu\bar{\nu}} = \frac{4G_F}{\sqrt{2}} \frac{\alpha_e}{2\pi s_W^2} \sum_{\ell=e,\mu,\tau} (V_{ts}^* V_{td} X^\ell + V_{cs}^* V_{cd} X_{\text{NL}}^\ell) (\bar{s} \gamma_\mu P_L d) (\bar{\nu}_\ell \gamma^\mu P_L \nu_\ell) + \text{h.c.} \quad (28)$$

In the SM, similar to the $b \rightarrow s\nu\bar{\nu}$ transition, the Z -penguin and W -box diagrams with internal top quark result in a flavour-universal Wilson coefficient $X_{\text{SM}}^\ell = X(x_t)$, with the Inami-Lim function $X(x_t)$ introduced already in eq. (16). The contribution from internal charm quark is represented by the function X_{NL}^ℓ . In the Z' scenario II, the Z' boson can only interact with the ν_μ neutrino. Its contributions to the operators with ν_e and ν_τ neutrinos arise from two-loop level and can be therefore neglected, i.e., $X_{\text{NP,II}}^e = X_{\text{NP,II}}^\tau = 0$. However, the Z' -penguin diagrams similar to the one shown in figure 4 contribute to the Wilson coefficient X^μ , and we

find $X_{\text{NP,II}}^\mu = -Y_{\text{NP}}^{\text{II}}$. In the Z' scenario I, as in the case of the $b \rightarrow s\nu\bar{\nu}$ transition, the Z' effects arise firstly at two-loop level and are neglected, i.e., $X_{\text{NP,I}}^\ell = 0$.

In the SM, with the help of isospin symmetry, the branching ratio of $K^+ \rightarrow \pi^+\nu\bar{\nu}$ decay after summing over the three neutrino flavours is given by [113–115]

$$\mathcal{B}(K^+ \rightarrow \pi^+\nu\bar{\nu}) = \frac{1}{3}\kappa_+(1 + \Delta_{\text{EM}}) \sum_{\ell=e,\mu,\tau} \left[\left(\frac{\text{Im}[\lambda_t X^\ell]}{\lambda^5} \right)^2 + \left(\frac{\text{Re}\lambda_c}{\lambda} P_c(X) + \frac{\text{Re}[\lambda_t X^\ell]}{\lambda^5} \right)^2 \right]. \quad (29)$$

The parameter κ_+ contains the relevant hadronic matrix elements extracted from the $K_{\ell 3}$ decays, and numerically we have $\kappa_+ = (5.173 \pm 0.025) \times 10^{-11} (\lambda/0.225)^8$ [97]. The parameter $\Delta_{\text{EM}} = -0.003$ describes the isospin breaking correction [114, 115]. The parameter $P_c(X)$ summarizes the SD charm contribution [95, 107, 116, 117] and the long-distance contributions [118]. Numerically, it is found that $P_c(X) = 0.404 \pm 0.024$ [97].

The rare decay $K_L \rightarrow \pi^0\nu\bar{\nu}$ proceeds in the SM almost entirely through direct CP violation [119, 120]. It is completely dominated by the SD loop diagrams with top-quark exchanges, and the charm contribution can be fully neglected [113]. With the help of isospin symmetry, the branching ratio of $K_L \rightarrow \pi^0\nu\bar{\nu}$ decay after summing over three neutrino flavours reads [113, 121]

$$\mathcal{B}(K_L \rightarrow \pi^0\nu\bar{\nu}) = \frac{1}{3}\kappa_L(1 - \delta_\epsilon) \sum_{\ell=e,\mu,\tau} \left(\frac{1}{\lambda^5} \text{Im}[\lambda_t X^\ell] \right)^2, \quad (30)$$

where κ_L encodes the hadronic matrix element extracted from the $K_{\ell 3}$ data [114, 122], and numerically $\kappa_L = (2.231 \pm 0.013) \times 10^{-10} (\lambda/0.225)^8$. The parameter δ_ϵ denotes the indirectly CP-violating contribution, and is highly suppressed by the $K^0 - \bar{K}^0$ mixing parameter $|\epsilon|$ [120].

3.6 $t \rightarrow c\mu^+\mu^-$ decay

In the SM, the rare FCNC decay $t \rightarrow c\mu^+\mu^-$ is highly suppressed by the Glashow-Iliopoulos-Maiani mechanism [123], with a branching ratio of $\mathcal{O}(10^{-10})$ [124, 125]. However, this process could be significantly enhanced by the Z' boson through the tree-level diagrams shown in figure 5. Let us discuss the Z' effects in the cases $m_{Z'} > m_t$ and $m_{Z'} < m_t$, respectively.

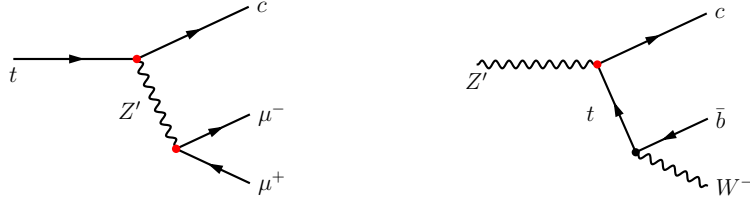


Figure 5: Feynman diagrams for the $t \rightarrow c\mu^+\mu^-$ (left) and $Z' \rightarrow \bar{b}cW^-$ (right) decays in the Z' scenarios.

3.6.1 $m_{Z'} > m_t$

The branching ratio of the Z' -mediated $t \rightarrow c\mu^+\mu^-$ decay can be written as

$$\mathcal{B}(t \rightarrow c\mu^+\mu^-) = \frac{\Gamma(t \rightarrow c\mu^+\mu^-)}{\Gamma_t}, \quad (31)$$

where Γ_t is the total width of the top quark. The differential decay width can be calculated from the left tree-level diagram shown in figure 5, with the result in the Z' scenario I given by

$$\frac{d\Gamma_0^I(t \rightarrow c\mu^+\mu^-)}{dq^2} = \frac{|X_{ct}^L \lambda_{\mu\mu}^L|^2 (m_t^2 - q^2)(m_t^4 + q^2 m_t^2 - 2q^4)}{768\pi^3 m_t^3 (q^2 - m_{Z'}^2)^2 + m_{Z'}^2 \Gamma_{Z'}^2}, \quad (32)$$

where q^2 denotes the dilepton invariant mass squared, and $\Gamma_{Z'}$ the finite decay width of the Z' boson. Since the Z' boson cannot be on-shell in the case of $m_{Z'} > m_t$, we can safely neglect the finite-width effect of the Z' boson here. After including the NLO QCD correction, the differential decay width of $t \rightarrow c\mu^+\mu^-$ can be rewritten as

$$\frac{d\Gamma_{\text{NLO}}^I(t \rightarrow c\mu^+\mu^-)}{dq^2} = \frac{d\Gamma_0^I(t \rightarrow c\mu^+\mu^-)}{dq^2} [1 + f_{\text{NLO}}(q^2)], \quad (33)$$

where the factor $f_{\text{NLO}}(q^2)$ can be obtained from the NLO QCD calculation of the $t \rightarrow cZ$ decay [126–128], and is given explicitly by

$$f_{\text{NLO}}(q^2) = \frac{4\alpha_s}{3\pi} \left[-\frac{1}{2}\pi^2 - 3 - \frac{1}{2} \log \frac{\mu^2}{m_t^2} + \frac{12 + 135\beta^2 - 43\beta^4}{12\beta^2(3 - \beta^2)} + \left(2 \log \beta - \frac{9 - \beta^2}{3 - \beta^2} \right) \log \beta \right. \\ \left. + \frac{(1 - \beta^2)(1 - 4\beta^2 + \beta^4)}{\beta^4(3 - \beta^2)} \log(1 - \beta^2) + \text{Li}_2(\beta^2) + \text{Li}_2(1 - \beta^{-2}) \right], \quad (34)$$

with $\beta = \sqrt{1 - q^2/m_t^2}$. Numerically, the NLO QCD corrections decrease the LO width by 6.4% \sim 9.1% for $m_t < m_{Z'} < 1$ TeV. Expressions in scenario II can be obtained from the above formulas with the replacement $(X_{ct}^L, \lambda_{\mu\mu}^L) \rightarrow (X_{23}^L, \lambda_{22}^L)$. As will be shown in subsection 4.2.2, the branching ratio $\mathcal{B}(t \rightarrow c\mu^+\mu^-)$ is predicted to be below $\mathcal{O}(10^{-5})$ in the two Z' scenarios. Therefore, their contributions to the top-quark total width Γ_t can be safely neglected.

3.6.2 $m_{Z'} < m_t$

In the case of $m_{Z'} < m_t$, the branching ratio of the Z' -mediated $t \rightarrow c\mu^+\mu^-$ decay can also be written as eqs. (32) and (33). However, since the intermediate Z' boson can be on-shell in this case, it is necessary to consider the Z' finite-width effect in eq. (32). When $m_W < m_{Z'} < m_t$, the main Z' decay modes in scenario I are $Z' \rightarrow \mu^+\mu^-$ and $Z' \rightarrow b\bar{c}W^+$ decays. Therefore, the total width of the Z' boson can be written as

$$\Gamma_{Z'}^I = \Gamma^I(Z' \rightarrow \mu^+\mu^-) + 2\Gamma^I(Z' \rightarrow b\bar{c}W^+), \quad (35)$$

where the decay width of $Z' \rightarrow \mu^+\mu^-$ is given by

$$\Gamma^I(Z' \rightarrow \mu^+\mu^-) = \frac{1}{24\pi} |\lambda_{\mu\mu}^L|^2 m_{Z'}, \quad (36)$$

and the width of the top-quark mediated $Z' \rightarrow b\bar{c}W^+$ decay reads

$$\begin{aligned} \Gamma^I(Z' \rightarrow b\bar{c}W^+) = & \frac{G_F |V_{tb}|^2 |X_{ct}|^2 m_t^8}{128\sqrt{2}\pi^3 m_{Z'}^5} \left\{ 4y_W^3 y_{Z'}^3 \log \frac{y_{Z'}}{y_W} + \frac{1}{12}(y_{Z'} - y_W) \left[60 + 48y_W^2 y_{Z'}^2 \right. \right. \\ & + 20y_W y_{Z'} + (30 - 39y_W y_{Z'})(y_W + y_{Z'}) - 88(y_W^2 + y_{Z'}^2) + 9(y_W^3 + y_{Z'}^3) \left. \right] \\ & \left. + \left[5 + 9y_W^2 y_{Z'}^2 - 9(y_W^2 + y_{Z'}^2) - 4y_W^3 y_{Z'}^3 + 4(y_W^3 + y_{Z'}^3) \right] \log \frac{\beta_{Z'}}{\beta_W^2} \right\}, \quad (37) \end{aligned}$$

with $\beta_W = \sqrt{1 - m_W^2/m_t^2}$, $\beta_{Z'} = \sqrt{1 - m_{Z'}^2/m_t^2}$, $y_W = m_W^2/m_t^2$, and $y_{Z'} = m_{Z'}^2/m_t^2$.

In scenario II, the Z' boson can also decay into the additional channels $Z' \rightarrow \nu_\mu \bar{\nu}_\mu$ and $Z' \rightarrow b\bar{s}$. The total width can then be written as

$$\Gamma_{Z'}^{II} = \Gamma^{II}(Z' \rightarrow \mu^+\mu^-) + \Gamma^{II}(Z' \rightarrow \nu_\mu \bar{\nu}_\mu) + 2\Gamma^{II}(Z' \rightarrow \bar{c}bW^+) + 2\Gamma^{II}(Z' \rightarrow b\bar{s}), \quad (38)$$

with

$$\Gamma^{II}(Z' \rightarrow \nu_\mu \bar{\nu}_\mu) = \frac{1}{24\pi} |\lambda_{22}^L|^2 m_{Z'} \quad \text{and} \quad \Gamma^{II}(Z' \rightarrow b\bar{s}) = \frac{1}{8\pi} |X_{23}^L|^2 m_{Z'}. \quad (39)$$

The decay widths $\Gamma^{II}(Z' \rightarrow \mu^+\mu^-)$ and $\Gamma^{II}(Z' \rightarrow \bar{c}bW^+)$ can be obtained from eqs. (36) and (37) with the replacement $(\lambda_{\mu\mu}^L, X_{ct}^L) \rightarrow (\lambda_{22}^L, X_{23}^L)$.

In the SM, $t \rightarrow bW$ is the main decay channel of the top quark. When $m_{Z'} < m_t$, the top quark can also decay into an on-shell Z' , which contributes to the top-quark total width as

$$\Gamma_t \simeq \Gamma(t \rightarrow bW) + \Gamma(t \rightarrow cZ'). \quad (40)$$

After including the NLO QCD correction, we can write the decay width of $t \rightarrow bW$ as [129–131]

$$\Gamma(t \rightarrow bW) = \Gamma_0(t \rightarrow bW) \left\{ 1 + \frac{2\alpha_s}{3\pi} \left[2 \left(\frac{(1 - \beta_W^2)(2\beta_W^2 - 1)(\beta_W^2 - 2)}{\beta_W^4(3 - 2\beta_W^2)} \right) \log(1 - \beta_W^2) - \frac{9 - 4\beta_W^2}{3 - 2\beta_W^2} \log \beta_W^2 + 2\text{Li}_2\beta_W^2 - 2\text{Li}_2(1 - \beta_W^2) - \frac{6\beta_W^4 - 3\beta_W^2 - 8}{2\beta_W^2(3 - 2\beta_W^2)} - \pi^2 \right] \right\}, \quad (41)$$

with the LO result given by

$$\Gamma_0(t \rightarrow bW) = \frac{G_F m_t^3}{8\sqrt{2}\pi} |V_{tb}|^2 \beta_W^4 (3 - 2\beta_W^2). \quad (42)$$

For the $t \rightarrow cZ'$ decay in scenario I, the decay width including the NLO QCD correction can be written as

$$\Gamma_{\text{NLO}}^{\text{I}}(t \rightarrow cZ') = \Gamma_0^{\text{I}}(t \rightarrow cZ') [1 + f_{\text{NLO}}(m_{Z'}^2)], \quad (43)$$

with the tree-level result given by

$$\Gamma_0^{\text{I}}(t \rightarrow cZ') = \frac{m_t^3}{32\pi m_{Z'}^2} |X_{ct}|^2 \beta_{Z'}^4 (3 - 2\beta_{Z'}^2). \quad (44)$$

The factor $f_{\text{NLO}}(q^2)$ is obtained from the calculation of NLO QCD correction to the $t \rightarrow cZ$ decay [126–128] and its explicit expression has been given in eq. (34). Numerically, we find $f(m_{Z'}^2) \approx -10.7\% \sim +5.3\%$ when $m_{Z'}$ varies in the range $105 \text{ GeV} < m_{Z'} < m_t$. Expressions in the Z' scenario II can be obtained from the above formulas with the replacement $(X_{ct}^L, \lambda_{\mu\mu}^L) \rightarrow (X_{23}^L, \lambda_{22}^L)$. Since the decay rate of $t \rightarrow cZ'$ is proportional to $|X_{ct}^L|^2$ in scenario I, the top-quark width can provide a unique constraint on the $t\bar{c}Z'$ coupling in the case of $m_{Z'} < m_t$.

4 Numerical results and discussions

In this section, we proceed to present our numerical analysis of the Z' scenarios presented in section 2. In table 1, we list the main input parameters used throughout this work. Table 2 summaries the SM predictions and the current experimental data for the various processes discussed in the previous section.

As discussed in section 2, the relevant model parameters in Z' scenario I (II) contain the complex couplings X_{ct}^L and $\lambda_{\mu\mu}^L$ (X_{23}^L and λ_{22}^L), and the Z' mass $m_{Z'}$. When performing a global

Input	Value	Unit	Ref.
m_t^{pole}	173.76 ± 0.30	GeV	[132]
$m_b(m_b)$	4.195 ± 0.014	GeV	[133]
$m_c(m_c)$	1.273 ± 0.01	GeV	[133]
$ V_{cb} (\text{semi-leptonic})$	$(41.1 \pm 0.3 \pm 0.5) \times 10^{-3}$		[134]
$ V_{ub} (\text{semi-leptonic})$	$(3.91 \pm 0.08 \pm 0.21) \times 10^{-3}$		[134]
$ V_{us} f_+^{K \rightarrow \pi}(0)$	0.2165 ± 0.0004		[134]
γ	$72.1_{-5.7}^{+5.4}$	°	[134]
$f_+^{K \rightarrow \pi}(0)$	$0.9681 \pm 0.0014 \pm 0.0022$		[134]

Table 1: Main input parameters used in our numerical analysis.

Observable	SM	Exp.	Ref.
$\mathcal{B}(B_s \rightarrow \mu^+ \mu^-)$	$(3.46 \pm 0.11) \times 10^{-9}$	$(3.09_{-0.43-0.11}^{+0.46+0.15}) \times 10^{-9}$	[21]
Δm_s [GeV]	$(1.18 \pm 0.07) \times 10^{-11}$	$(1.1688 \pm 0.0014) \times 10^{-11}$	[135]
$S_{\psi\phi}$	0.041 ± 0.003	0.033 ± 0.033	[135]
$\mathcal{B}(B \rightarrow X_s \nu \bar{\nu})$	$(3.03 \pm 0.08) \times 10^{-5}$	$< 6.4 \times 10^{-4}$	[136]
$\mathcal{B}(B^+ \rightarrow K^+ \nu \bar{\nu})$	$(4.15 \pm 0.56) \times 10^{-6}$	$< 1.9 \times 10^{-5}$	[137]
$\mathcal{B}(B^0 \rightarrow K^0 \nu \bar{\nu})$	$(3.85 \pm 0.52) \times 10^{-6}$	$< 2.6 \times 10^{-5}$	[137]
$\mathcal{B}(B^+ \rightarrow K^{*+} \nu \bar{\nu})$	$(9.71 \pm 0.93) \times 10^{-6}$	$< 6.1 \times 10^{-5}$	[137]
$\mathcal{B}(B^0 \rightarrow K^{*0} \nu \bar{\nu})$	$(9.01 \pm 0.87) \times 10^{-6}$	$< 1.8 \times 10^{-5}$	[137]
$\mathcal{B}(K_L \rightarrow \mu^+ \mu^-)$	$(7.34 \pm 1.21) \times 10^{-9}$	$(6.84 \pm 0.11) \times 10^{-9}$	[132]
$\mathcal{B}(K_S \rightarrow \mu^+ \mu^-)$	$(5.18 \pm 1.57) \times 10^{-12}$	$(0.94_{-0.64}^{+0.72}) \times 10^{-10}$	[138]
$\mathcal{B}(K^+ \rightarrow \pi^+ \nu \bar{\nu})$	$(8.38 \pm 0.62) \times 10^{-11}$	$(10.6_{-3.4}^{+4.0} \pm 0.9) \times 10^{-11}$	[139]
$\mathcal{B}(K_L \rightarrow \pi^0 \nu \bar{\nu})$	$(3.46 \pm 0.46) \times 10^{-11}$	$< 3.0 \times 10^{-9}$	[140]

Table 2: Our SM predictions and the experimental measurements of the relevant observables used in our global fit. Upper limits are all at 95% confidence level (CL) .

fit on these parameters and studying their effects, we consider the following parameter space:

$$\begin{aligned}
\text{S.I:} \quad & |X_{ct}^L| < 2.0, \quad |\lambda_{\mu\mu}^L| < 2.0, \quad 105 \text{ GeV} < m_{Z'} < 1000 \text{ GeV}, \\
\text{S.II:} \quad & |X_{23}^L| < 2.0, \quad |\lambda_{22}^L| < 2.0, \quad 105 \text{ GeV} < m_{Z'} < 1000 \text{ GeV},
\end{aligned} \tag{45}$$

where the upper limits on the magnitudes of the couplings correspond to about half of the perturbativity bound $\sqrt{4\pi}$. Here the lower bound of $m_{Z'}$ is chosen to avoid the potentially

strong bound from the branching ratio $\mathcal{B}(t \rightarrow cZ)$ [141] (see subsection 4.2.2 for further details).

In our numerical analysis, we follow the approach used in ref. [86] and construct a likelihood function that only depends on the Wilson coefficients as

$$-2 \log L(\mathbf{C}) = \sum_i \mathbf{x}_i^T(\mathbf{C}) [V_{\text{exp}} + V_{\text{th}}(\boldsymbol{\theta})]^{-1} \mathbf{x}_i(\mathbf{C}), \quad (46)$$

with the definition

$$\mathbf{x}_i(\mathbf{C}) = \mathcal{O}_i^{\text{exp}} - \mathcal{O}_i^{\text{th}}(\mathbf{C}, \boldsymbol{\theta}).$$

Here, $\mathcal{O}_i^{\text{exp}}$ are the central values of the experimental measurements, while $\mathcal{O}_i^{\text{th}}$ denote the central values of the theoretical predictions, which depend on the Wilson coefficients \mathbf{C} and the input parameters $\boldsymbol{\theta}$. V_{exp} is the covariance matrix of the experimental measurements, while V_{th} denotes the covariance matrix of the theoretical predictions, which contains all the theoretical uncertainties and their correlations. Generally, the covariance matrix V_{th} depends on both the Wilson coefficients \mathbf{C} and the input parameters $\boldsymbol{\theta}$. However, as all the experimental measurements do not show large deviations from the SM predictions, we have neglected in our numerical analysis the dependence of V_{th} on the Z' contributions to the Wilson coefficients \mathbf{C} , i.e., V_{th} is evaluated with the Wilson coefficients \mathbf{C} fixed to their SM values. Furthermore, the theoretical uncertainties are approximated as Gaussian and obtained by randomly sampling the observables with the input parameters $\boldsymbol{\theta}$ distributed according to their probability density functions. With eq. (46), the $\Delta\chi^2$ function, which depends on the Wilson coefficients \mathbf{C} , can be written as $\Delta\chi^2(\mathbf{C}) = -2 \log L(\mathbf{C})/L_{\text{max}}$, where L_{max} denotes the maximum of L at different values of the Wilson coefficients. For more details on the fit methodology, we refer to refs. [86, 142]. Our global fit is performed using an extended version of the package `flavio` [142].

4.1 Flavour constraints

As discussed in section 3, the Z' contributions to the $b \rightarrow s\mu^+\mu^-$, $s \rightarrow d\mu^+\mu^-$, $b \rightarrow s\nu\bar{\nu}$, and $s \rightarrow d\nu\bar{\nu}$ transitions are all controlled by the products $X_{ct}^L \lambda_{\mu\mu}^L / m_{Z'}^2$, in scenario I or $X_{23}^L \lambda_{22}^L / m_{Z'}^2$, in scenario II. These two products are complex in general and constraints on them will be derived in terms of their real and imaginary parts in the following analysis.

For the $b \rightarrow s\mu^+\mu^-$ transitions, as in refs. [27, 143–145], we consider the following experimen-

tal data in the numerical analysis: 1) the branching ratios of the decays $B \rightarrow K\mu^+\mu^-$ [146], $B \rightarrow K^*\mu^+\mu^-$ [146–149], $B_s \rightarrow \phi\mu^+\mu^-$ [16], $\Lambda_b \rightarrow \Lambda\mu^+\mu^-$ [150], $B \rightarrow X_s\mu^+\mu^-$ [151], and $B_s \rightarrow \mu^+\mu^-$ [21]. 2) the angular distributions in $B \rightarrow K\mu^+\mu^-$ [147, 152], $B \rightarrow K^*\mu^+\mu^-$ [29, 30, 148, 153–155], $B_s \rightarrow \phi\mu^+\mu^-$ [156], and $\Lambda_b \rightarrow \Lambda\mu^+\mu^-$ [157] decays. 3) the LFU ratios $R_{K^{(*)}}$ [9–11, 13–15]. In scenarios I and II, the best fit regions of the Z' parameters in terms of their real and imaginary parts are shown in figure 6. The best fit values in scenario I (II) read $\text{Re}X_{ct}^L\lambda_{\mu\mu}^L/m_{Z'}^2 = 0.0991$ and $\text{Im}X_{ct}^L\lambda_{\mu\mu}^L/m_{Z'}^2 = -0.184$ ($\text{Re}X_{23}^L\lambda_{22}^L/m_{Z'}^2 = -0.0007$ and $\text{Im}X_{23}^L\lambda_{22}^L/m_{Z'}^2 = 0.0018$) in unit of TeV^{-2} with $\text{Pull}_{\text{SM}} = 4.91\sigma$ (4.96σ), which is defined as $\sqrt{\Delta\chi^2}$ between the best fit point and the SM value [145]. We observe that both the Z' scenarios I and II allow a good description of the current $b \rightarrow s\mu^+\mu^-$ measurements. This is not surprising, because the Z' scenarios considered induce NP effects along the direction $\mathcal{C}_9^{\text{NP}} = -\mathcal{C}_{10}^{\text{NP}}$, which is strongly preferred in the model-independent global fit [27, 28, 31, 143–145, 158–161]. In the survived parameter space of the scenarios I and II, the magnitude of $X_{ct}^L\lambda_{\mu\mu}^L/m_{Z'}^2$ and $X_{23}^L\lambda_{22}^L/m_{Z'}^2$ are of $\mathcal{O}(10^{-1})\text{TeV}^{-2}$ and $\mathcal{O}(10^{-3})\text{TeV}^{-2}$, respectively. In both of these two scenarios, the real parts of $X_{ct}^L\lambda_{\mu\mu}^L/m_{Z'}^2$ and $X_{23}^L\lambda_{22}^L/m_{Z'}^2$ are bounded from below, while the imaginary parts are loosely constrained. It is noted that the $b \rightarrow s\mu^+\mu^-$ decays provide the most stringent constraints on the Z' parameters among all the flavour processes, as will be discussed in the following.

The rare decays $K_L \rightarrow \mu^+\mu^-$ and $K_S \rightarrow \mu^+\mu^-$ are induced by the $s \rightarrow d\mu^+\mu^-$ transition. In the Z' scenarios, the constraints from the branching ratios $\mathcal{B}(K_{L,S} \rightarrow \mu^+\mu^-)_{\text{SD}}$ are shown in figure 7. As discussed in subsection 3.3, the Z' boson in scenarios I and II affects the $s \rightarrow d\mu^+\mu^-$ transition via the same penguin diagram. Therefore, the constraints on the Z' parameters are identical in the two scenarios, as shown in figure 7. It can also be seen that the bounds on the imaginary parts of $X_{ct}^L\lambda_{\mu\mu}^L/m_{Z'}^2$ and $X_{23}^L\lambda_{22}^L/m_{Z'}^2$ are quite weak. In addition, the constraints from the $s \rightarrow d\mu^+\mu^-$ decays, while being relatively weaker compared to that from the $b \rightarrow s\mu^+\mu^-$ decays, are still compatible with the parameter regions required to explain the $b \rightarrow s\mu^+\mu^-$ anomalies shown in figure 6.

Since the Z' boson does not couple directly to the neutrinos in the Z' scenario I, the $b \rightarrow s\nu\bar{\nu}$ and $s \rightarrow d\nu\bar{\nu}$ decays are not relevant for this scenario. In the Z' scenario II, on the other hand, the Z' boson affects the $b \rightarrow s\nu\bar{\nu}$ and $s \rightarrow d\nu\bar{\nu}$ transitions at the tree and the one-loop level,

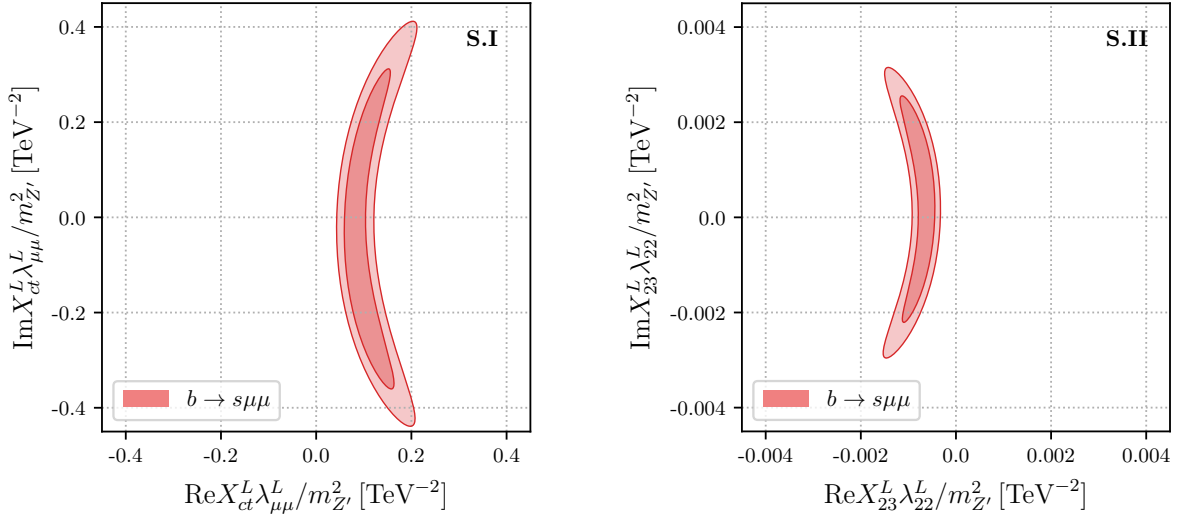


Figure 6: Allowed regions of the real and imaginary parts of $X_{ct}^L \lambda_{\mu\mu}^L / m_{Z'}^2$ and $X_{23}^L \lambda_{22}^L / m_{Z'}^2$ by the $b \rightarrow s \mu^+ \mu^-$ processes in the Z' scenarios I (left) and II (right). The dark and the light regions correspond to the 68% and the 95% CL, respectively.

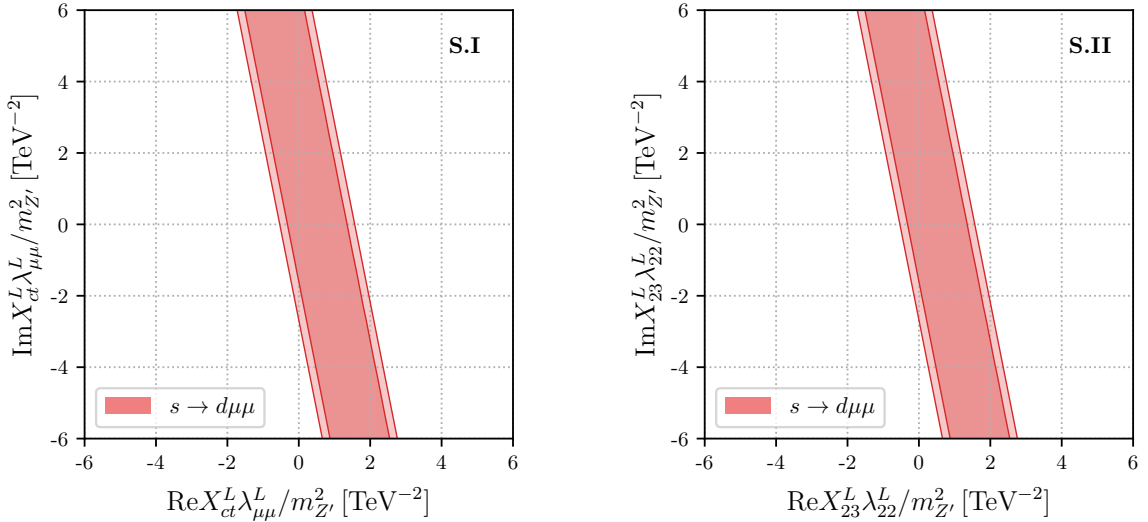


Figure 7: Same as in figure 6 but now under the constraints from the $s \rightarrow d \mu^+ \mu^-$ processes.

respectively. In order to constrain the Z' parameters, we consider five $b \rightarrow s \nu \bar{\nu}$ processes (i.e., the decays $B \rightarrow X_s \nu \bar{\nu}$, $B^0 \rightarrow K^{(*)0} \nu \bar{\nu}$, and $B^+ \rightarrow K^{(*)+} \nu \bar{\nu}$), and two $s \rightarrow d \nu \bar{\nu}$ processes (i.e., the decays $K^+ \rightarrow \pi^+ \nu \bar{\nu}$ and $K_L \rightarrow \pi^0 \nu \bar{\nu}$). We show in figure 8 the allowed regions of the real and imaginary parts of $X_{23}^L \lambda_{22}^L / m_{Z'}^2$ by the branching ratios of these decays. It can be seen that the bound from the $s \rightarrow d \nu \bar{\nu}$ decays is much weaker than that from the $b \rightarrow s \nu \bar{\nu}$ transitions. This can be understood by the fact that the Z' contributions to the former is suppressed by

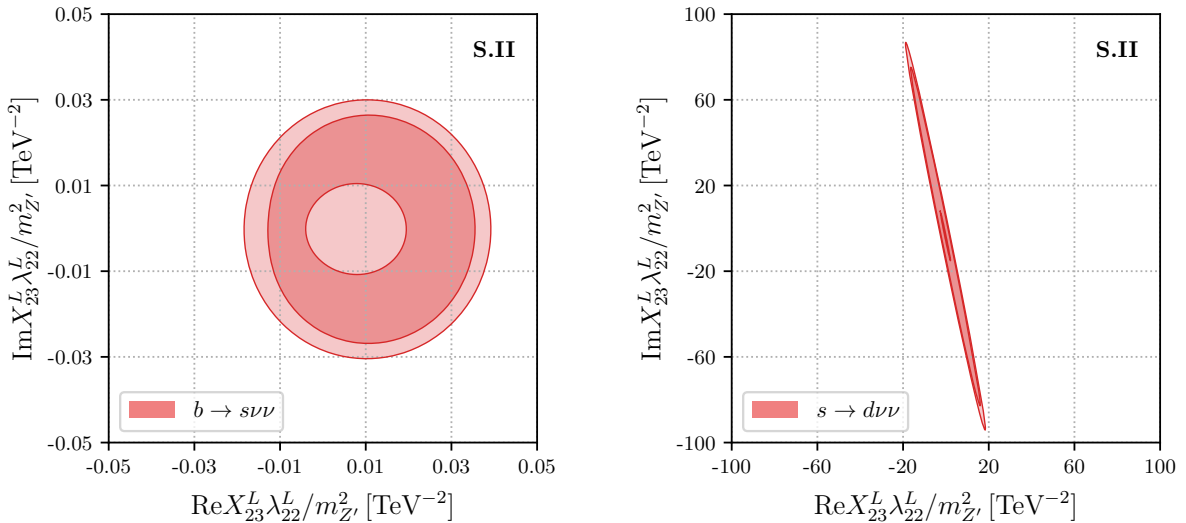


Figure 8: Allowed regions of the real and imaginary parts of $X_{23}^L \lambda_{22}^L / m_{Z'}^2$, by the $b \rightarrow s \nu \bar{\nu}$ (left) and $s \rightarrow d \nu \bar{\nu}$ processes (right) in scenario II. The colour captions are the same as in figure 6.

$\mathcal{O}(\lambda^3)$ while its contributions to the latter do not suffer any CKM suppression. In addition, the constraints from the $b \rightarrow s \nu \bar{\nu}$ and $s \rightarrow d \nu \bar{\nu}$ decays are consistent with the best fit region from the $b \rightarrow s \mu^+ \mu^-$ processes.

In the Z' scenario I, as explained in subsection 3.2, the $B_s - \bar{B}_s$ mixing cannot provide any relevant constraint on the Z' parameters. In the Z' scenario II, the Z' contribution is proportional to the product $(X_{23}^L)^2 / m_{Z'}^2$, due to the tree-level Z' exchange. After taking into account the constraints from the mass difference Δm_s and the CP-violating observable $S_{\psi\phi}$, we obtain the allowed regions in the plane $(\text{Re} X_{23}^L / m_{Z'}, \text{Im} X_{23}^L / m_{Z'})$, which are shown in figure 9. It can be seen that the mass difference Δm_s provides a strong bound on $\text{Re} X_{23}^L / m_{Z'}$. For $\text{Im} X_{23}^L / m_{Z'}$, the bound arises mainly from the CP-violating observable $S_{\psi\phi}$ and is weaker compared to the one on $\text{Re} X_{23}^L / m_{Z'}$, due to the currently larger experimental uncertainty of $S_{\psi\phi}$. The phase of the maximum value of $|X_{23}^L| / m_{Z'}$ also matches the CKM phase β_s [134].

Summarizing the numerical analysis made above, we can see that the strongest constraints are provided by the $b \rightarrow s \mu^+ \mu^-$ processes in the Z' scenario I. Therefore, after considering all the flavour processes, we can obtain the combined allowed regions from figure 6, with the numerical results given by

$$0.04 < \frac{\text{Re} X_{ct}^L \lambda_{\mu\mu}^L}{m_{Z'}^2} < 0.21 \text{ TeV}^{-2}, \quad -0.44 < \frac{\text{Im} X_{ct}^L \lambda_{\mu\mu}^L}{m_{Z'}^2} < 0.41 \text{ TeV}^{-2}, \quad (47)$$

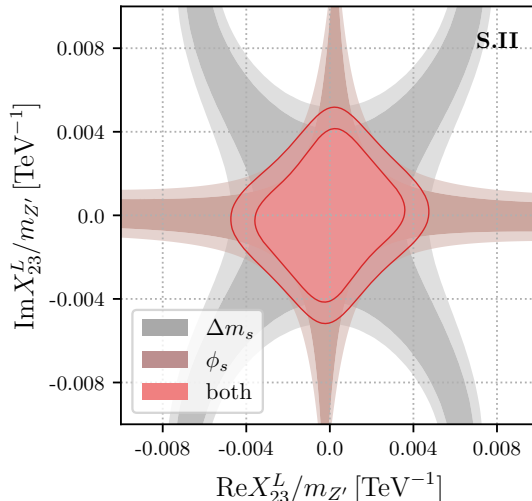


Figure 9: Allowed regions in the plane $(\text{Re}X_{23}^L/m_{Z'}, \text{Im}X_{23}^L/m_{Z'})$ by the $B_s - \bar{B}_s$ mixing in the Z' scenario II. The dark and the light regions correspond to the 68% and the 95% CL, respectively.

at the 95% CL. The above lower bound on $\text{Re}X_{ct}^L \lambda_{\mu\mu}^L/m_{Z'}^2$, together with the parameter space chosen in eq. (45), implies an upper bound on the Z' mass, $m_{Z'} < 9.0 \text{ TeV}$.

Turning to the Z' scenario II, the $b \rightarrow s\mu^+\mu^-$ processes also provide the most stringent constraints on the Z' parameter, as in scenario I. Therefore, after considering all the B - and K -meson FCNC decays, the combined constraints can be obtained from figure 6, and numerically

$$-0.0015 < \frac{\text{Re}X_{23}^L \lambda_{22}^L}{m_{Z'}^2} < -0.0003 \text{ TeV}^{-2}, \quad -0.0029 < \frac{\text{Im}X_{23}^L \lambda_{22}^L}{m_{Z'}^2} < +0.0031 \text{ TeV}^{-2}, \quad (48)$$

at the 95% CL. However, different from the scenario I, the $B_s - \bar{B}_s$ mixing also provides an independent bound on the parameter product $X_{23}^L/m_{Z'}$. Numerically, the combined constraints shown in figure 9 correspond to

$$-0.004 < \frac{\text{Re}X_{23}^L}{m_{Z'}} < +0.004 \text{ TeV}^{-1}, \quad -0.005 < \frac{\text{Im}X_{23}^L}{m_{Z'}} < +0.005 \text{ TeV}^{-1}, \quad (49)$$

at the 95% CL. In the case of $\lambda_{22}^L/m_{Z'} \sim \mathcal{O}(1) \text{ TeV}^{-1}$, constraints on $X_{23}^L/m_{Z'}$ from the $b \rightarrow s\mu^+\mu^-$ processes and the $B_s - \bar{B}_s$ mixing are of the same order. Furthermore, since $\text{Re}X_{23}^L \lambda_{22}^L/m_{Z'}^2$ is lower bounded by the $b \rightarrow s\mu^+\mu^-$ processes, a lower bound, $\lambda_{22}^L/m_{Z'} > 0.07 \text{ TeV}^{-1}$, can be derived in order to simultaneously satisfy the constraints from the $B_s - \bar{B}_s$ mixing. Therefore, the Z' couplings in scenario II exhibit the hierarchy $\lambda_{22}^L \gg X_{23}^L$. Finally, our numerical analysis has shown that the main constraints in scenario II are obtained from the

processes affected by the tree-level Z' contributions. Therefore, the flavour phenomenology of the Z' scenario II is almost identical to that of the minimal Z' scenario discussed in refs. [34, 45].

4.2 Collider constraints

In this subsection, we discuss the collider constraints on the Z' scenarios in the case of both $m_{Z'} > m_t$ and $m_{Z'} < m_t$. For recent collider studies of similar Z' scenarios with top-FCNC couplings, we refer to refs. [162–164].

4.2.1 $m_{Z'} > m_t$

In the case of $m_{Z'} > m_t$, constraints on the Z' parameters could be obtained from the decay $t \rightarrow c\mu^+\mu^-$. However, the current LHC searches for the decay $t \rightarrow c\mu^+\mu^-$ have been only performed at the Z peak, with $|m_{\mu^+\mu^-} - m_Z| < 15$ GeV, and interpreted as a bound on $\mathcal{B}(t \rightarrow cZ)$ [141, 165–167]. No dedicated searches for non-resonant (outside the Z peak) $t \rightarrow c\mu^+\mu^-$ decays have been performed yet. In ref. [168], an upper bound on $\mathcal{B}(t \rightarrow c\mu^+\mu^-)$ was estimated by using the experimental bounds on $\mathcal{B}(t \rightarrow cZ)$ and $\mathcal{B}(Z \rightarrow \mu^+\mu^-) = 3.37\%$ [132]. With such an approach, an upper bound $\mathcal{B}(t \rightarrow c\mu^+\mu^-) < 4.4 \times 10^{-6}$ can be derived from the current bound $\mathcal{B}(t \rightarrow cZ) < 1.3 \times 10^{-4}$ set by the ATLAS experiment with an integrated luminosity of 139 fb^{-1} at 13 TeV [141]. In this way, constraints on the Z' parameters can be derived from the bound $\mathcal{B}(t \rightarrow c\mu^+\mu^-) < 4.4 \times 10^{-6}$. However, we find that such a constraint is at least one order of magnitude weaker than that obtained from the low-energy flavour processes discussed in the last subsection.

Within the effective field theory (EFT) framework, by using different signal regions of the LHC searches for the rare FCNC decay $t \rightarrow cZ$, an improved approach has been developed in ref. [169]. However, in the case when $m_{Z'}$ is not far from m_t , the framework with four-fermion effective operators is not appropriate to describe the Z' contributions to the decay $t \rightarrow c\mu^+\mu^-$.

4.2.2 $m_{Z'} < m_t$

In the case of $m_{Z'} < m_t$, the $t \rightarrow c\mu^+\mu^-$ decay involves the resonant Z' contribution, and is expected to provide strong constraints on the Z' parameters. However, similar to the case of $m_{Z'} > m_t$, no experimental searches for the $t \rightarrow c\mu^+\mu^-$ decay mediated by the Z' resonance has

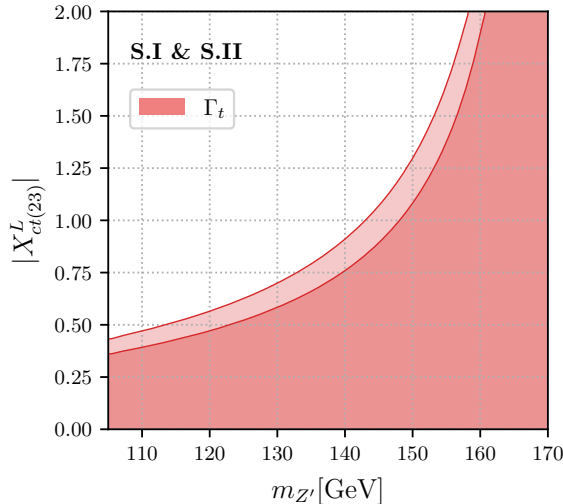


Figure 10: Allowed regions in the plane $(|X_{ct(23)}^L|, m_{Z'})$ from the top-quark width Γ_t in the Z' scenario I (II). The colour captions are the same as in figure 6.

been performed yet. Detailed analysis of the signal shape could be used to derive constraints from the current $\mathcal{B}(t \rightarrow cZ)$ bound, as performed in ref. [169]. Especially, for $|m_{Z'} - m_Z| < 15$ GeV, the signal regions of the $t \rightarrow cZ$ and $t \rightarrow cZ'$ decays can be largely overlapped, and stringent constraints on the Z' parameters could be therefore derived. We leave these possibilities for further work, and concentrate on the mass region $105 \text{ GeV} < m_{Z'} < m_t$ to avoid the potentially strong bound from $\mathcal{B}(t \rightarrow cZ)$ [141].

As discussed in subsection 3.6.2, in the case of $m_{Z'} < m_t$, the decay $t \rightarrow cZ'$ can contribute to the top-quark width. Compared to the SM prediction $\Gamma_t^{\text{SM}} = 1.3 \text{ GeV}$ [170], the current measurement $\Gamma_t = (1.42^{+0.19}_{-0.15}) \text{ GeV}$ [132] leaves $\mathcal{O}(20\%)$ room for the Z' effects. We show in figure 10 the allowed regions in the plane $(|X_{ct(23)}^L|, m_{Z'})$ in the scenario I (II). For scenario I, it is noted that the top-quark width provides a unique bound on the coupling X_{ct}^L . For scenario II, the bound on X_{23}^L is much weaker than that obtained from the $B_s - \bar{B}_s$ mixing.

4.3 Predictions

As mentioned in the last subsection, experimental searches for the $t \rightarrow c\mu^+\mu^-$ decay off the Z pole have not been performed yet. Using the allowed parameter space derived in the global fit, we can make prediction on the branching ratio $\mathcal{B}(t \rightarrow c\mu^+\mu^-)$ in the two Z' scenarios as a function of the Z' mass, which is shown in figure 11. Although there are several studies of the

expected sensitivities to the $t \rightarrow cZ$ decay at the LHC [171] and other future colliders [172–174], to our knowledge, detailed analysis of the $t \rightarrow c\mu^+\mu^-$ decay at the LHC has not been performed yet. In order to estimate the current (future) experimental sensitivity to $\mathcal{B}(t \rightarrow c\mu^+\mu^-)$, we adopt as a benchmark the product of $\mathcal{B}(Z \rightarrow \mu^+\mu^-) = 3.37\%$ [132] and the current (future projected) experimental limit on $\mathcal{B}(t \rightarrow cZ)$. With the current ATLAS limit $\mathcal{B}(t \rightarrow cZ) < 1.3 \times 10^{-4}$ based on the full Run-2 data [141] and the future expected sensitivity 5×10^{-5} at the HL-LHC with 3 ab^{-1} [171], the current and the future sensitivity to $\mathcal{B}(t \rightarrow c\mu^+\mu^-)$ are estimated to be 4.4×10^{-6} and 1.7×10^{-6} respectively, as shown by the dashed and the dotted line in figure 11. Here we make the following two observations:

- In the case of $m_{Z'} < m_t$, the branching ratio of $t \rightarrow c\mu^+\mu^-$ decay in the two Z' scenarios is strongly enhanced by the resonance effect, which is several orders of magnitude higher than the one in the case of $m_{Z'} > m_t$. In the mass region $105 \text{ GeV} < m_{Z'} < m_t$, the predicted $\mathcal{B}(t \rightarrow c\mu^+\mu^-)$ in scenario I (II) is higher (lower) than the current and future estimated bounds. Therefore, experimental searches for the $t \rightarrow c\mu^+\mu^-$ decay are expected to probe a Z' mass window of $[105 \text{ GeV}, m_t]$.
- In the case of $m_{Z'} > m_t$, the predicted $\mathcal{B}(t \rightarrow c\mu^+\mu^-)$ in scenario I is compatible with the estimated sensitivities, while the one in scenario II is several orders of magnitude lower than the estimated future sensitivity. Therefore, direct searches for the decay in scenario II with a heavy Z' boson could be very challenging for the LHC and its high-luminosity upgrade.

Besides the $t \rightarrow c\mu^+\mu^-$ decay, which should be searched in $pp \rightarrow t\bar{t}$ production, the associated production $pp \rightarrow tZ'$ could also be considered and may provide more relevant constraints for a heavy Z' boson. Recently, the associated production of a single top with dileptons has been investigated in the EFT framework [175], and a 95% CL bound on the scale of the effective operator $(\bar{t}\gamma^\mu P_L c)(\bar{\mu}\gamma_\mu P_L \mu)$, $\Lambda_{tc\mu\mu} = 1.1 (1.5) \text{ TeV}$, has been obtained at the LHC with an integrated luminosity of $140 (3000) \text{ fb}^{-1}$. In the Z' scenario I (II) with $m_{Z'} = 1 \text{ TeV}$, the 95% CL allowed parameter space in our global fit results in $1.4 (17.0) < \Lambda_{tc\mu\mu} < 4.8 (55.2) \text{ TeV}$. This implies that the Z' scenario I reaches the sensitivity of the HL-LHC even for a TeV-scale Z' boson.² Detailed collider simulation is still necessary to obtain more reliable estimation of the

²In the Z' scenario II, the $b\bar{s}Z'$ coupling makes the $pp \rightarrow \mu^+\mu^-$ process sensitive to the Z' boson. For more

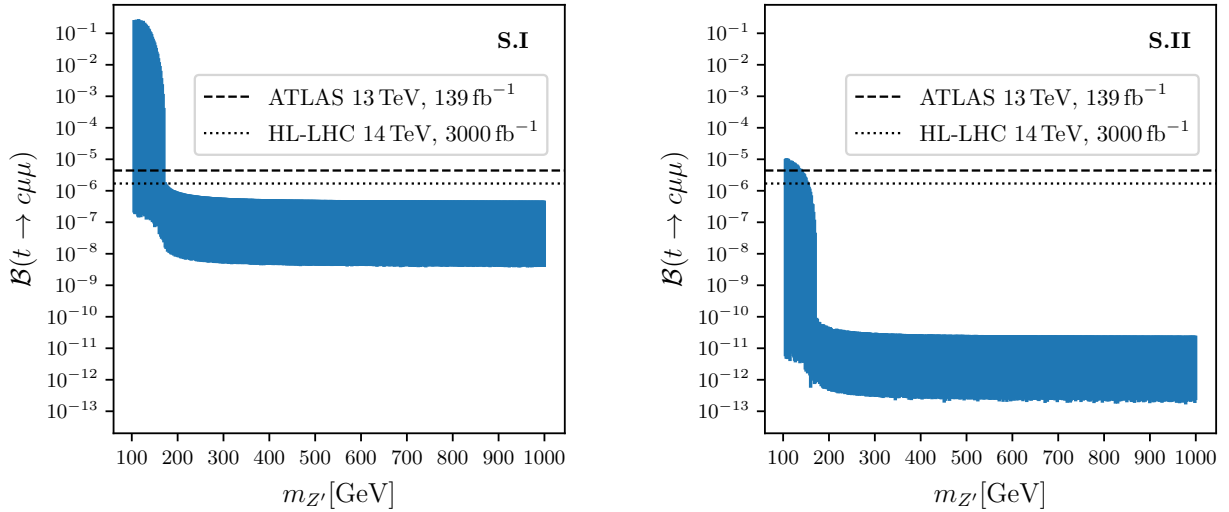


Figure 11: The branching ratio of $t \rightarrow c\mu^+\mu^-$ decay as a function of $m_{Z'}$ in the Z' scenarios I (left) and II (right). The dark regions are allowed at the 95% CL.

experimental sensitivity, which will be our future work. We also encourage our experimental colleagues to carry out relevant searches for such a Z' boson.

An important feature of our Z' scenarios is that the Z' contributions to all the FCNC decays are controlled by the same product, $X_{ct}^L \lambda_{\mu\mu}^L / m_{Z'}^2$ in scenario I or $X_{23}^L \lambda_{22}^L / m_{Z'}^2$ in scenario II. Therefore, all the B - and K -meson processes are strongly correlated. As an illustration, we show in figure 12 the correlations among some observables. From these plots, we make the following two observations:

- The branching ratio $\mathcal{B}(K_L \rightarrow \mu^+\mu^-)$ is suppressed by the Z' effects in scenario I. However, its SM value remain almost unchanged in scenario II, due to the strongly constrained Z' couplings. For the $B^0 \rightarrow K^{*0}\mu^+\mu^-$ decay, the situation is opposite: the branching ratio is enhanced in scenario II, while remaining unchanged in scenario I. These correlations can be used to distinguish the two Z' scenarios. In addition, the Z' effects on the branching ratios of $K_S \rightarrow \mu^+\mu^-$, $K_L \rightarrow \pi\nu\bar{\nu}$ and $K^+ \rightarrow \pi^+\nu\bar{\nu}$ decays are all found to be negligible in the two scenarios and will be not shown here.
- The correlations between $R_K^{[1.1, 6.0]}$ and $R_{K^*}^{[1.1, 6.0]}$, which are the LFU ratios in the q^2 bin $[1.1, 6.0]$ GeV², as well as the correlations between $R_{K^*}^{[1.1, 6.0]}$ and P'_5 , in the two Z' scenarios are almost identical. The reason is that the best fit regions for the Wilson coefficients \mathcal{C}_9

details, we refer to ref. [52].

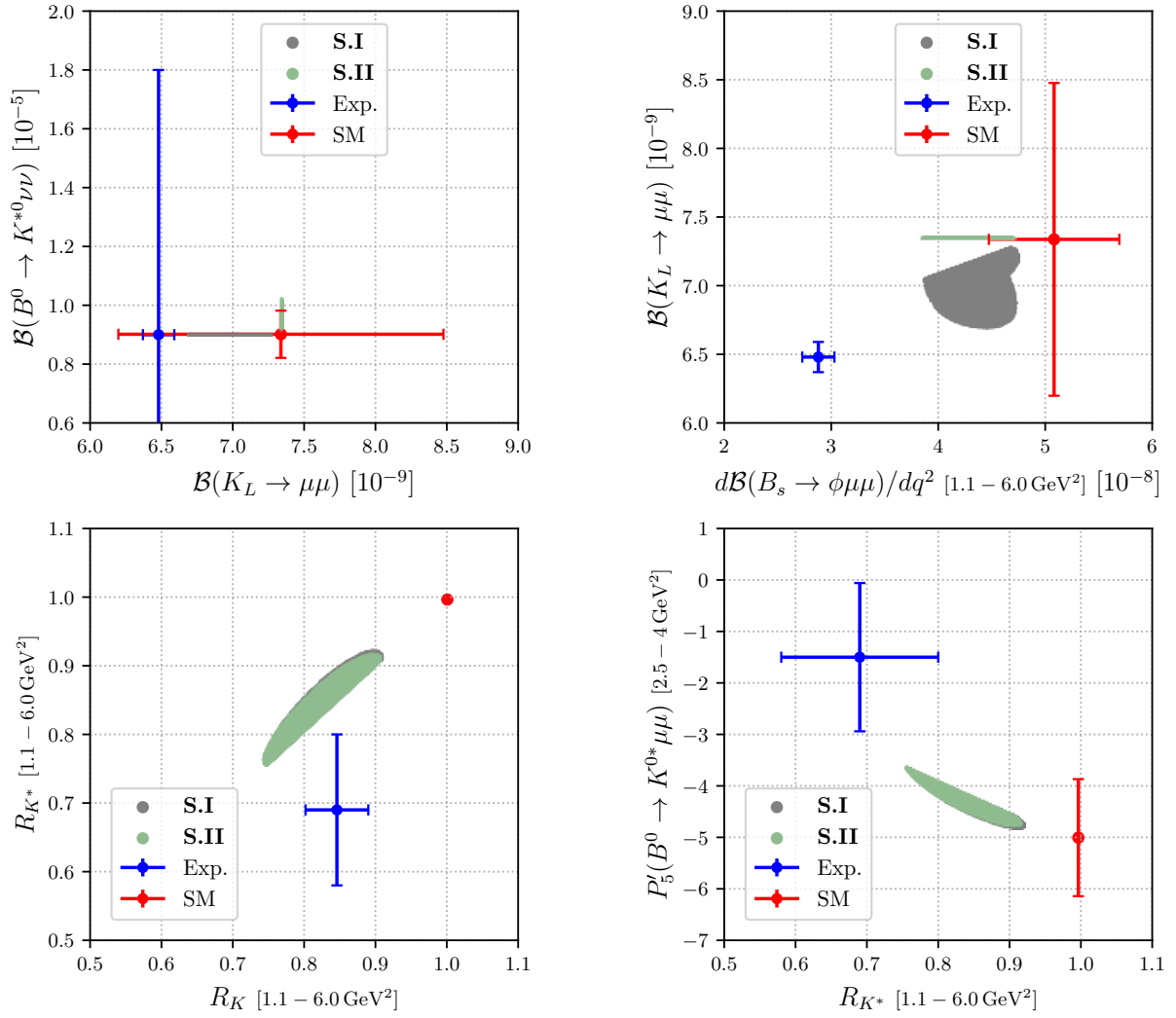


Figure 12: Correlations between the observables of B - and K -meson decays in the two Z' scenarios. The 1σ range of the experimental measurements and the SM predictions are shown, except the data on $\mathcal{B}(B^0 \rightarrow K^{*0} \nu \nu)$, which corresponds to the 90% CL limit.

and \mathcal{C}_{10} are numerically almost the same in the two scenarios. As expected, the Z' effects make $R_{K^{(*)}}^{[1.1, 6.0]}$, P'_5 , and $\mathcal{B}(B_s \rightarrow \phi \mu^+ \mu^-)$ move closer to the experimental measurements.

With high-precision measurements at the HL-LHC and Belle II [176], these interesting correlation could provide further insights into our Z' scenarios.

In the case of $m_{Z'} \gg m_t$, the Z' contributions to both the $t \rightarrow c \mu^+ \mu^-$ and $b \rightarrow s \mu^+ \mu^-$ processes are controlled by the same products, $X_{ct}^L \lambda_{\mu\mu}^L / m_{Z'}^2$ in scenario I or $X_{23}^L \lambda_{22}^L / m_{Z'}^2$ in scenario II, since they are described by the effective $t\bar{c}\mu^+\mu^-$ operator. Thus, we show in figure 13 the correlation between $R_{K^{(*)}}^{[1.1, 6.0]}$ and $\mathcal{B}(t \rightarrow c \mu^+ \mu^-)$ for $m_{Z'} = 1 \text{ TeV}$. It can be seen

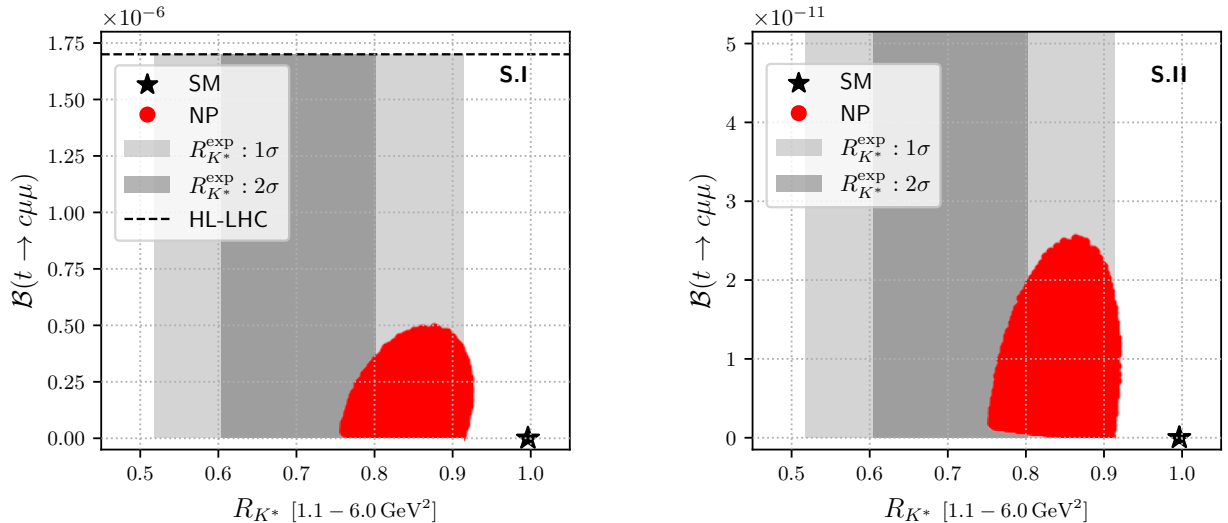


Figure 13: Correlation between R_{K^*} and $\mathcal{B}(t \rightarrow c\mu^+\mu^-)$ in the Z' scenarios I (left) and II (right) for $m_{Z'} = 1$ TeV with real (gray) and complex (red) couplings.

that $\mathcal{B}(t \rightarrow c\mu^+\mu^-)$ approaches to its maximum value when $R_{K^*}^{[1.1, 6.0]} \approx 0.85$. The predicted upper limit is of the same order as the estimated future LHC sensitivity in scenario I, while being quite below the estimated sensitivity in scenario II.

5 Conclusions

Motivated by the recent anomalies in the $b \rightarrow s\ell^+\ell^-$ transitions, we have considered a phenomenological Z' scenario (denoted as scenario I), in which a heavy Z' boson couples only to $t\bar{c}$ and $\mu^+\mu^-$ with left-handed chirality. The Z' effects on the $b \rightarrow s\mu^+\mu^-$ processes automatically induce opposite contributions to the effective operators \mathcal{O}_9 and \mathcal{O}_{10} , which is favored by the model-independent analyses of the $b \rightarrow s\ell^+\ell^-$ anomalies.

We have performed a global fit to all relevant experimental data. It is found that such a minimal Z' scenario can address the current $b \rightarrow s\ell^+\ell^-$ anomalies, while simultaneously satisfying other flavour and collider constraints. The mass of the Z' boson can be less than 1 TeV. In the region $105 \text{ GeV} < m_{Z'} < m_t$, the $t \rightarrow c\mu^+\mu^-$ decay is significantly enhanced by resonance effects and can serve as a sensitive probe of such a Z' boson. As an important feature of this scenario, all the low-energy flavour observables are controlled by the product $X_{ct}^L \lambda_{\mu\mu}^L / m_{Z'}^2$. We have found interesting correlations among the various flavour observables,

which could provide further insights into this scenario.

We have also considered an extended scenario (denoted as scenario II), in which the Z' boson interacts with the $SU_L(2)$ fermion doublets with analogous couplings as in scenario I. Due to tree-level Z' contributions, the Z' couplings suffer from severe constraints from the $b \rightarrow s\ell^+\ell^-$ processes and the $B_s-\bar{B}_s$ mixing, which makes the collider signals of $t \rightarrow c\mu^+\mu^-$ decay below the estimated sensitivity at the HL-LHC. The correlations between flavour observables in scenario II are different from that observed in scenario I, and can be therefore used to distinguish between the two scenarios.

Our scenarios can be modified by replacing $t\bar{c}Z'$ with $t\bar{u}Z'$ coupling. Then the K -meson rare decays could become more relevant due to the large CKM factors involved, and the tZ' associated production at the LHC may play crucial role in searching for such a Z' boson. A right-handed $\mu^+\mu^-Z'$ coupling can also be taken into account to simultaneously accommodate the $(g-2)_\mu$ anomaly. In addition, if the $\mu^+\mu^-Z'$ coupling is replaced by the e^+e^-Z' coupling, the direct production of the Z' boson at e^+e^- collider should then be taken into account. It is noted that, although our Z' scenarios are not realistic, our studies have shown that a vector boson with top-quark FCNC interactions can explain the current $b \rightarrow s\ell^+\ell^-$ anomalies and may provide new avenues for model buildings. We also encourage our experimental colleagues to carry out relevant searches for such a Z' boson at the LHC and its high-luminosity upgrade.

Acknowledgements

This work is supported by the National Natural Science Foundation of China under Grant Nos. 12135006, 12075097, 11675061, 11775092, and 11805077, as well as by the self-determined research funds of CCNU from the colleges' basic research and operation of MOE under Grant Nos. CCNU19TD012 and CCNU20TS007. XY is also supported in part by the Startup Research Funding from CCNU.

References

- [1] Y. Li and C.-D. Lü, *Recent Anomalies in B Physics*, *Sci. Bull.* **63** (2018) 267–269, [arXiv:1808.02990].

- [2] S. Bifani, S. Descotes-Genon, A. Romero Vidal, and M.-H. Schune, *Review of Lepton Universality tests in B decays*, *J. Phys. G* **46** (2019), no. 2 023001, [arXiv:1809.06229].
- [3] J. Albrecht, D. van Dyk, and C. Langenbruch, *Flavour anomalies in heavy quark decays*, *Prog. Part. Nucl. Phys.* **120** (2021) 103885, [arXiv:2107.04822].
- [4] D. London and J. Matias, *B Flavour Anomalies: 2021 Theoretical Status Report*, arXiv:2110.13270.
- [5] G. Hiller and F. Kruger, *More model-independent analysis of $b \rightarrow s$ processes*, *Phys. Rev. D* **69** (2004) 074020, [hep-ph/0310219].
- [6] **HPQCD** Collaboration, C. Bouchard, G. P. Lepage, C. Monahan, H. Na, and J. Shigemitsu, *Standard Model Predictions for $B \rightarrow K\ell^+\ell^-$ with Form Factors from Lattice QCD*, *Phys. Rev. Lett.* **111** (2013), no. 16 162002, [arXiv:1306.0434]. [Erratum: *Phys.Rev.Lett.* 112, 149902 (2014)].
- [7] M. Bordone, G. Isidori, and A. Pattori, *On the Standard Model predictions for R_K and R_{K^*}* , *Eur. Phys. J. C* **76** (2016), no. 8 440, [arXiv:1605.07633].
- [8] G. Isidori, S. Nabeebaccus, and R. Zwicky, *QED corrections in $\bar{B} \rightarrow \bar{K}\ell^+\ell^-$ at the double-differential level*, *JHEP* **12** (2020) 104, [arXiv:2009.00929].
- [9] **LHCb** Collaboration, R. Aaij et al., *Test of lepton universality in beauty-quark decays*, arXiv:2103.11769.
- [10] **LHCb** Collaboration, R. Aaij et al., *Search for lepton-universality violation in $B^+ \rightarrow K^+\ell^+\ell^-$ decays*, *Phys. Rev. Lett.* **122** (2019), no. 19 191801, [arXiv:1903.09252].
- [11] **LHCb** Collaboration, R. Aaij et al., *Test of lepton universality with $B^0 \rightarrow K^{*0}\ell^+\ell^-$ decays*, *JHEP* **08** (2017) 055, [arXiv:1705.05802].
- [12] **LHCb** Collaboration, R. Aaij et al., *Tests of lepton universality using $B^0 \rightarrow K_S^0\ell^+\ell^-$ and $B^+ \rightarrow K^{*+}\ell^+\ell^-$ decays*, arXiv:2110.09501.
- [13] **BaBar** Collaboration, J. P. Lees et al., *Measurement of Branching Fractions and Rate Asymmetries in the Rare Decays $B \rightarrow K^{(*)}l^+l^-$* , *Phys. Rev. D* **86** (2012) 032012, [arXiv:1204.3933].
- [14] **Belle** Collaboration, A. Abdesselam et al., *Test of lepton flavor universality in $B \rightarrow K^*\ell^+\ell^-$ decays at Belle*, arXiv:1904.02440.
- [15] **BELLE** Collaboration, S. Choudhury et al., *Test of lepton flavor universality and search for lepton flavor violation in $B \rightarrow K\ell\ell$ decays*, *JHEP* **03** (2021) 105, [arXiv:1908.01848].
- [16] **LHCb** Collaboration, R. Aaij et al., *Branching fraction measurements of the rare $B_s^0 \rightarrow \phi\mu^+\mu^-$ and $B_s^0 \rightarrow f_2'(1525)\mu^+\mu^-$ decays*, arXiv:2105.14007.

- [17] R. R. Horgan, Z. Liu, S. Meinel, and M. Wingate, *Calculation of $B^0 \rightarrow K^{*0} \mu^+ \mu^-$ and $B_s^0 \rightarrow \phi \mu^+ \mu^-$ observables using form factors from lattice QCD*, *Phys. Rev. Lett.* **112** (2014) 212003, [[arXiv:1310.3887](#)].
- [18] R. R. Horgan, Z. Liu, S. Meinel, and M. Wingate, *Rare B decays using lattice QCD form factors*, *PoS LATTICE2014* (2015) 372, [[arXiv:1501.00367](#)].
- [19] A. Bharucha, D. M. Straub, and R. Zwicky, *$B \rightarrow V \ell^+ \ell^-$ in the Standard Model from light-cone sum rules*, *JHEP* **08** (2016) 098, [[arXiv:1503.05534](#)].
- [20] N. Rajeev, N. Sahoo, and R. Dutta, *Angular analysis of $B_s \rightarrow f_2'(1525) (\rightarrow K^+ K^-) \mu^+ \mu^-$ decays as a probe to lepton flavor universality violation*, *Phys. Rev. D* **103** (2021), no. 9 095007, [[arXiv:2009.06213](#)].
- [21] **LHCb** Collaboration, R. Aaij et al., *Analysis of neutral B-meson decays into two muons*, [arXiv:2108.09284](#).
- [22] **ATLAS, CMS and LHCb** Collaboration, ATLAS, CMS, and LHCb, *Combination of the ATLAS, CMS and LHCb results on the $B_{(s)}^0 \rightarrow \mu^+ \mu^-$ decays*, .
- [23] C. Bobeth, M. Gorbahn, T. Hermann, M. Misiak, E. Stamou, and M. Steinhauser, *$B_{s,d} \rightarrow l^+ l^-$ in the Standard Model with Reduced Theoretical Uncertainty*, *Phys. Rev. Lett.* **112** (2014) 101801, [[arXiv:1311.0903](#)].
- [24] M. Beneke, C. Bobeth, and R. Szafron, *Power-enhanced leading-logarithmic QED corrections to $B_q \rightarrow \mu^+ \mu^-$* , *JHEP* **10** (2019) 232, [[arXiv:1908.07011](#)].
- [25] **ATLAS** Collaboration, M. Aaboud et al., *Study of the rare decays of B_s^0 and B^0 mesons into muon pairs using data collected during 2015 and 2016 with the ATLAS detector*, *JHEP* **04** (2019) 098, [[arXiv:1812.03017](#)].
- [26] **CMS** Collaboration, A. M. Sirunyan et al., *Measurement of properties of $B_s^0 \rightarrow \mu^+ \mu^-$ decays and search for $B^0 \rightarrow \mu^+ \mu^-$ with the CMS experiment*, *JHEP* **04** (2020) 188, [[arXiv:1910.12127](#)].
- [27] W. Altmannshofer and P. Stangl, *New Physics in Rare B Decays after Moriond 2021*, [arXiv:2103.13370](#).
- [28] L.-S. Geng, B. Grinstein, S. Jäger, S.-Y. Li, J. Martin Camalich, and R.-X. Shi, *Implications of new evidence for lepton-universality violation in $b \rightarrow s \ell^+ \ell^-$ decays*, [arXiv:2103.12738](#).
- [29] **LHCb** Collaboration, R. Aaij et al., *Measurement of CP-Averaged Observables in the $B^0 \rightarrow K^{*0} \mu^+ \mu^-$ Decay*, *Phys. Rev. Lett.* **125** (2020), no. 1 011802, [[arXiv:2003.04831](#)].
- [30] **LHCb** Collaboration, R. Aaij et al., *Angular Analysis of the $B^+ \rightarrow K^{*+} \mu^+ \mu^-$ Decay*, *Phys. Rev. Lett.* **126** (2021), no. 16 161802, [[arXiv:2012.13241](#)].

- [31] M. Ciuchini, M. Fedele, E. Franco, A. Paul, L. Silvestrini, and M. Valli, *Lessons from the $B^{0,+} \rightarrow K^{*0,+} \mu^+ \mu^-$ angular analyses*, *Phys. Rev. D* **103** (2021), no. 1 015030, [arXiv:2011.01212].
- [32] T. Hurth, F. Mahmoudi, and S. Neshatpour, *Implications of the new LHCb angular analysis of $B \rightarrow K^* \mu^+ \mu^-$: Hadronic effects or new physics?*, *Phys. Rev. D* **102** (2020), no. 5 055001, [arXiv:2006.04213].
- [33] N. Gubernari, D. van Dyk, and J. Virto, *Non-local matrix elements in $B_{(s)} \rightarrow \{K^{(*)}, \phi\} \ell^+ \ell^-$* , *JHEP* **02** (2021) 088, [arXiv:2011.09813].
- [34] R. Gauld, F. Goertz, and U. Haisch, *On minimal Z' explanations of the $B \rightarrow K^* \mu^+ \mu^-$ anomaly*, *Phys. Rev. D* **89** (2014) 015005, [arXiv:1308.1959].
- [35] A. J. Buras and J. Girrbach, *Left-handed Z' and Z FCNC quark couplings facing new $b \rightarrow s \mu^+ \mu^-$ data*, *JHEP* **12** (2013) 009, [arXiv:1309.2466].
- [36] W. Altmannshofer, S. Gori, M. Pospelov, and I. Yavin, *Quark flavor transitions in $L_\mu - L_\tau$ models*, *Phys. Rev. D* **89** (2014) 095033, [arXiv:1403.1269].
- [37] A. Crivellin, G. D'Ambrosio, and J. Heeck, *Explaining $h \rightarrow \mu^\pm \tau^\mp$, $B \rightarrow K^* \mu^+ \mu^-$ and $B \rightarrow K \mu^+ \mu^- / B \rightarrow K e^+ e^-$ in a two-Higgs-doublet model with gauged $L_\mu - L_\tau$* , *Phys. Rev. Lett.* **114** (2015) 151801, [arXiv:1501.00993].
- [38] A. Crivellin, G. D'Ambrosio, and J. Heeck, *Addressing the LHC flavor anomalies with horizontal gauge symmetries*, *Phys. Rev. D* **91** (2015), no. 7 075006, [arXiv:1503.03477].
- [39] A. Crivellin, L. Hofer, J. Matias, U. Nierste, S. Pokorski, and J. Rosiek, *Lepton-flavour violating B decays in generic Z' models*, *Phys. Rev. D* **92** (2015), no. 5 054013, [arXiv:1504.07928].
- [40] A. Celis, J. Fuentes-Martin, M. Jung, and H. Serodio, *Family nonuniversal Z' models with protected flavor-changing interactions*, *Phys. Rev. D* **92** (2015), no. 1 015007, [arXiv:1505.03079].
- [41] G. Bélanger, C. Delaunay, and S. Westhoff, *A Dark Matter Relic From Muon Anomalies*, *Phys. Rev. D* **92** (2015) 055021, [arXiv:1507.06660].
- [42] A. Falkowski, M. Nardecchia, and R. Ziegler, *Lepton Flavor Non-Universality in B -meson Decays from a $U(2)$ Flavor Model*, *JHEP* **11** (2015) 173, [arXiv:1509.01249].
- [43] B. Allanach, F. S. Queiroz, A. Strumia, and S. Sun, *Z' models for the LHCb and $g - 2$ muon anomalies*, *Phys. Rev. D* **93** (2016), no. 5 055045, [arXiv:1511.07447]. [Erratum: Phys.Rev.D 95, 119902 (2017)].
- [44] P. Ko, Y. Omura, Y. Shigekami, and C. Yu, *LHCb anomaly and B physics in flavored*

- Z'* models with flavored Higgs doublets, *Phys. Rev. D* **95** (2017), no. 11 115040, [arXiv:1702.08666].
- [45] S. Di Chiara, A. Fowlie, S. Fraser, C. Marzo, L. Marzola, M. Raidal, and C. Spethmann, *Minimal flavor-changing Z' models and muon $g - 2$ after the R_{K^*} measurement*, *Nucl. Phys. B* **923** (2017) 245–257, [arXiv:1704.06200].
- [46] C. Bonilla, T. Modak, R. Srivastava, and J. W. F. Valle, *$U(1)_{B_3-3L_\mu}$ gauge symmetry as a simple description of $b \rightarrow s$ anomalies*, *Phys. Rev. D* **98** (2018), no. 9 095002, [arXiv:1705.00915].
- [47] J. Ellis, M. Fairbairn, and P. Tunney, *Anomaly-Free Models for Flavour Anomalies*, *Eur. Phys. J. C* **78** (2018), no. 3 238, [arXiv:1705.03447].
- [48] Y. Tang and Y.-L. Wu, *Flavor non-universal gauge interactions and anomalies in B-meson decays*, *Chin. Phys. C* **42** (2018), no. 3 033104, [arXiv:1705.05643]. [Erratum: Chin.Phys.C 44, 069101 (2020)].
- [49] S. F. King, *Flavourful Z' models for $R_{K^{(*)}}$* , *JHEP* **08** (2017) 019, [arXiv:1706.06100].
- [50] S. Baek, *Dark matter contribution to $b \rightarrow s\mu^+\mu^-$ anomaly in local $U(1)_{L_\mu-L_\tau}$ model*, *Phys. Lett. B* **781** (2018) 376–382, [arXiv:1707.04573].
- [51] S. F. King, *$R_{K^{(*)}}$ and the origin of Yukawa couplings*, *JHEP* **09** (2018) 069, [arXiv:1806.06780].
- [52] B. C. Allanach, T. Corbett, M. J. Dolan, and T. You, *Hadron collider sensitivity to fat flavourful Z's for $R_{K^{(*)}}$* , *JHEP* **03** (2019) 137, [arXiv:1810.02166].
- [53] B. C. Allanach and J. Davighi, *Naturalising the third family hypercharge model for neutral current B-anomalies*, *Eur. Phys. J. C* **79** (2019), no. 11 908, [arXiv:1905.10327].
- [54] W. Altmannshofer, J. Davighi, and M. Nardecchia, *Gauging the accidental symmetries of the standard model, and implications for the flavor anomalies*, *Phys. Rev. D* **101** (2020), no. 1 015004, [arXiv:1909.02021].
- [55] L. Calibbi, A. Crivellin, F. Kirk, C. A. Manzari, and L. Vernazza, *Z' models with less-minimal flavour violation*, *Phys. Rev. D* **101** (2020), no. 9 095003, [arXiv:1910.00014].
- [56] M. K. Mohapatra, N. Rajeev, and R. Dutta, *Combined analysis of $B_c \rightarrow D_s^{(*)}\mu^+\mu^-$ and $B_c \rightarrow D_s^{(*)}\nu\bar{\nu}$ decays within Z' and leptiquark new physics models*, arXiv:2108.10106.
- [57] V. M. Lozano, R. M. S. Seoane, and J. Zurita, *Z'-explorer 2.0: reconnoitering the dark matter landscape*, arXiv:2109.13194.
- [58] N. Rajeev and R. Dutta, *Consequences of $b \rightarrow s\mu^+\mu^-$ anomalies on $B \rightarrow K^{(*)}\nu\bar{\nu}$* ,

- $B_s \rightarrow (\eta, \eta') \nu \bar{\nu}$ and $B_s \rightarrow \phi \nu \bar{\nu}$ decay observables, [arXiv:2112.11682](#).
- [59] J. F. Kamenik, Y. Soreq, and J. Zupan, *Lepton flavor universality violation without new sources of quark flavor violation*, *Phys. Rev. D* **97** (2018), no. 3 035002, [[arXiv:1704.06005](#)].
- [60] P. J. Fox, I. Low, and Y. Zhang, *Top-philic Z' forces at the LHC*, *JHEP* **03** (2018) 074, [[arXiv:1801.03505](#)].
- [61] X.-Q. Li, Y.-D. Yang, and X.-B. Yuan, *Anomalous tqZ Coupling Effects in Rare B - and K -Meson Decays*, *JHEP* **03** (2012) 018, [[arXiv:1112.2674](#)].
- [62] H. Gong, Y.-D. Yang, and X.-B. Yuan, *Constraints on anomalous tcZ coupling from $\bar{B} \rightarrow \bar{K}^* \mu^+ \mu^-$ and $B_s \rightarrow \mu^+ \mu^-$ decays*, *JHEP* **05** (2013) 062, [[arXiv:1301.7535](#)].
- [63] R. Coy, M. Frigerio, F. Mescia, and O. Sumensari, *New physics in $b \rightarrow s \ell \ell$ transitions at one loop*, *Eur. Phys. J. C* **80** (2020), no. 1 52, [[arXiv:1909.08567](#)].
- [64] **Muon g-2** Collaboration, B. Abi et al., *Measurement of the Positive Muon Anomalous Magnetic Moment to 0.46 ppm*, *Phys. Rev. Lett.* **126** (2021), no. 14 141801, [[arXiv:2104.03281](#)].
- [65] T. Aoyama et al., *The anomalous magnetic moment of the muon in the Standard Model*, *Phys. Rept.* **887** (2020) 1–166, [[arXiv:2006.04822](#)].
- [66] G. Buchalla, A. J. Buras, and M. E. Lautenbacher, *Weak decays beyond leading logarithms*, *Rev. Mod. Phys.* **68** (1996) 1125–1144, [[hep-ph/9512380](#)].
- [67] C. Bobeth, P. Gambino, M. Gorbahn, and U. Haisch, *Complete NNLO QCD analysis of $\bar{B} \rightarrow X_s \ell^+ \ell^-$ and higher order electroweak effects*, *JHEP* **04** (2004) 071, [[hep-ph/0312090](#)].
- [68] T. Huber, E. Lunghi, M. Misiak, and D. Wyler, *Electromagnetic logarithms in $\bar{B} \rightarrow X_s \ell^+ \ell^-$* , *Nucl. Phys. B* **740** (2006) 105–137, [[hep-ph/0512066](#)].
- [69] T. Hermann, M. Misiak, and M. Steinhauser, *Three-loop QCD corrections to $B_s \rightarrow \mu^+ \mu^-$* , *JHEP* **12** (2013) 097, [[arXiv:1311.1347](#)].
- [70] C. Bobeth, M. Gorbahn, and E. Stamou, *Electroweak Corrections to $B_{s,d} \rightarrow \ell^+ \ell^-$* , *Phys. Rev. D* **89** (2014), no. 3 034023, [[arXiv:1311.1348](#)].
- [71] N. Cabibbo, *Unitary Symmetry and Leptonic Decays*, *Phys. Rev. Lett.* **10** (1963) 531–533.
- [72] M. Kobayashi and T. Maskawa, *CP Violation in the Renormalizable Theory of Weak Interaction*, *Prog. Theor. Phys.* **49** (1973) 652–657.
- [73] M. Beneke, T. Feldmann, and D. Seidel, *Exclusive radiative and electroweak $b \rightarrow d$ and*

- $b \rightarrow s$ penguin decays at NLO, *Eur. Phys. J. C* **41** (2005) 173–188, [hep-ph/0412400].
- [74] A. Khodjamirian, T. Mannel, A. A. Pivovarov, and Y. M. Wang, *Charm-loop effect in $B \rightarrow K^{(*)}\ell^+\ell^-$ and $B \rightarrow K^*\gamma$* , *JHEP* **09** (2010) 089, [arXiv:1006.4945].
- [75] M. Beylich, G. Buchalla, and T. Feldmann, *Theory of $B \rightarrow K^{(*)}\ell^+\ell^-$ decays at high q^2 : OPE and quark-hadron duality*, *Eur. Phys. J. C* **71** (2011) 1635, [arXiv:1101.5118].
- [76] C. Bobeth, G. Hiller, and D. van Dyk, *General analysis of $\bar{B} \rightarrow \bar{K}^{(*)}\ell^+\ell^-$ decays at low recoil*, *Phys. Rev. D* **87** (2013), no. 3 034016, [arXiv:1212.2321].
- [77] S. Jäger and J. Martin Camalich, *On $B \rightarrow V\ell\ell$ at small dilepton invariant mass, power corrections, and new physics*, *JHEP* **05** (2013) 043, [arXiv:1212.2263].
- [78] W. Altmannshofer, P. Ball, A. Bharucha, A. J. Buras, D. M. Straub, and M. Wick, *Symmetries and Asymmetries of $B \rightarrow K^*\mu^+\mu^-$ Decays in the Standard Model and Beyond*, *JHEP* **01** (2009) 019, [arXiv:0811.1214].
- [79] S. Descotes-Genon, T. Hurth, J. Matias, and J. Virto, *Optimizing the basis of $B \rightarrow K^*ll$ observables in the full kinematic range*, *JHEP* **05** (2013) 137, [arXiv:1303.5794].
- [80] Y. Aoki et al., *FLAG Review 2021*, arXiv:2111.09849.
- [81] P. Ball and R. Zwicky, *$B_{d,s} \rightarrow \rho, \omega, K^*, \phi$ decay form-factors from light-cone sum rules revisited*, *Phys. Rev. D* **71** (2005) 014029, [hep-ph/0412079].
- [82] N. Gubernari, A. Kokulu, and D. van Dyk, *$B \rightarrow P$ and $B \rightarrow V$ Form Factors from B -Meson Light-Cone Sum Rules beyond Leading Twist*, *JHEP* **01** (2019) 150, [arXiv:1811.00983].
- [83] C.-D. Lü, Y.-L. Shen, Y.-M. Wang, and Y.-B. Wei, *QCD calculations of $B \rightarrow \pi, K$ form factors with higher-twist corrections*, *JHEP* **01** (2019) 024, [arXiv:1810.00819].
- [84] J. Gao, C.-D. Lü, Y.-L. Shen, Y.-M. Wang, and Y.-B. Wei, *Precision calculations of $B \rightarrow V$ form factors from soft-collinear effective theory sum rules on the light-cone*, *Phys. Rev. D* **101** (2020), no. 7 074035, [arXiv:1907.11092].
- [85] Y.-L. Shen and Y.-B. Wei, *$B \rightarrow P, V$ form factors with the B -meson light-cone sum rules*, arXiv:2112.01500.
- [86] W. Altmannshofer and D. M. Straub, *New physics in $b \rightarrow s$ transitions after LHC run 1*, *Eur. Phys. J. C* **75** (2015), no. 8 382, [arXiv:1411.3161].
- [87] S. Descotes-Genon, L. Hofer, J. Matias, and J. Virto, *Global analysis of $b \rightarrow s\ell\ell$ anomalies*, *JHEP* **06** (2016) 092, [arXiv:1510.04239].
- [88] T. Blake, G. Lanfranchi, and D. M. Straub, *Rare B Decays as Tests of the Standard Model*, *Prog. Part. Nucl. Phys.* **92** (2017) 50–91, [arXiv:1606.00916].

- [89] A. J. Buras, S. Jager, and J. Urban, *Master formulae for Delta F=2 NLO QCD factors in the standard model and beyond*, *Nucl. Phys. B* **605** (2001) 600–624, [[hep-ph/0102316](#)].
- [90] A. J. Buras, M. Jamin, and P. H. Weisz, *Leading and Next-to-leading QCD Corrections to ϵ Parameter and $B^0 - \bar{B}^0$ Mixing in the Presence of a Heavy Top Quark*, *Nucl. Phys. B* **347** (1990) 491–536.
- [91] M. Ciuchini, E. Franco, V. Lubicz, G. Martinelli, I. Scimemi, and L. Silvestrini, *Next-to-leading order QCD corrections to Delta F = 2 effective Hamiltonians*, *Nucl. Phys. B* **523** (1998) 501–525, [[hep-ph/9711402](#)].
- [92] M. Artuso, G. Borissov, and A. Lenz, *CP violation in the B_s^0 system*, *Rev. Mod. Phys.* **88** (2016), no. 4 045002, [[arXiv:1511.09466](#)].
- [93] W. Altmannshofer, A. J. Buras, D. M. Straub, and M. Wick, *New strategies for New Physics search in $B \rightarrow K^* \nu \bar{\nu}$, $B \rightarrow K \nu \bar{\nu}$ and $B \rightarrow X_s \nu \bar{\nu}$ decays*, *JHEP* **04** (2009) 022, [[arXiv:0902.0160](#)].
- [94] A. J. Buras, J. Girrbach-Noe, C. Niehoff, and D. M. Straub, *$B \rightarrow K^{(*)} \nu \bar{\nu}$ decays in the Standard Model and beyond*, *JHEP* **02** (2015) 184, [[arXiv:1409.4557](#)].
- [95] G. Buchalla and A. J. Buras, *The rare decays $K \rightarrow \pi \nu \bar{\nu}$, $B \rightarrow X \nu \bar{\nu}$ and $B \rightarrow l^+ l^-$: An Update*, *Nucl. Phys. B* **548** (1999) 309–327, [[hep-ph/9901288](#)].
- [96] M. Misiak and J. Urban, *QCD corrections to FCNC decays mediated by Z penguins and W boxes*, *Phys. Lett. B* **451** (1999) 161–169, [[hep-ph/9901278](#)].
- [97] A. J. Buras, D. Buttazzo, J. Girrbach-Noe, and R. Knegjens, *$K^+ \rightarrow \pi^+ \nu \bar{\nu}$ and $K_L \rightarrow \pi^0 \nu \bar{\nu}$ in the Standard Model: status and perspectives*, *JHEP* **11** (2015) 033, [[arXiv:1503.02693](#)].
- [98] J. Brod, M. Gorbahn, and E. Stamou, *Two-Loop Electroweak Corrections for the $K \rightarrow \pi \nu \bar{\nu}$ Decays*, *Phys. Rev. D* **83** (2011) 034030, [[arXiv:1009.0947](#)].
- [99] T. Hurth, *Present status of inclusive rare B decays*, *Rev. Mod. Phys.* **75** (2003) 1159–1199, [[hep-ph/0212304](#)].
- [100] G. Buchalla and A. J. Buras, *QCD corrections to rare K and B decays for arbitrary top quark mass*, *Nucl. Phys. B* **400** (1993) 225–239.
- [101] Y. Grossman, Z. Ligeti, and E. Nardi, *New limit on inclusive $B \rightarrow X_s$ anti-neutrino neutrino decay and constraints on new physics*, *Nucl. Phys. B* **465** (1996) 369–398, [[hep-ph/9510378](#)]. [Erratum: *Nucl. Phys. B* **480**, 753–754 (1996)].
- [102] P. Colangelo, F. De Fazio, P. Santorelli, and E. Scrimieri, *Rare $B \rightarrow K^{(*)}$ neutrino anti-neutrino decays at B factories*, *Phys. Lett. B* **395** (1997) 339–344,

- [hep-ph/9610297].
- [103] **HPQCD** Collaboration, C. Bouchard, G. P. Lepage, C. Monahan, H. Na, and J. Shigemitsu, *Rare decay $B \rightarrow K\ell^+\ell^-$ form factors from lattice QCD*, *Phys. Rev. D* **88** (2013), no. 5 054509, [arXiv:1306.2384]. [Erratum: Phys.Rev.D 88, 079901 (2013)].
- [104] J. A. Bailey et al., *$B \rightarrow Kl^+l^-$ Decay Form Factors from Three-Flavor Lattice QCD*, *Phys. Rev. D* **93** (2016), no. 2 025026, [arXiv:1509.06235].
- [105] A. Khodjamirian and A. V. Rusov, *$B_s \rightarrow K\ell\nu_\ell$ and $B_{(s)} \rightarrow \pi(K)\ell^+\ell^-$ decays at large recoil and CKM matrix elements*, *JHEP* **08** (2017) 112, [arXiv:1703.04765].
- [106] R. R. Horgan, Z. Liu, S. Meinel, and M. Wingate, *Lattice QCD calculation of form factors describing the rare decays $B \rightarrow K^*\ell^+\ell^-$ and $B_s \rightarrow \phi\ell^+\ell^-$* , *Phys. Rev. D* **89** (2014), no. 9 094501, [arXiv:1310.3722].
- [107] G. Buchalla and A. J. Buras, *The rare decays $K^+ \rightarrow \pi^+\nu\bar{\nu}$ and $K_L \rightarrow \mu^+\mu^-$ beyond leading logarithms*, *Nucl. Phys. B* **412** (1994) 106–142, [hep-ph/9308272].
- [108] M. Gorbahn and U. Haisch, *Charm Quark Contribution to $K_L \rightarrow \mu^+\mu^-$ at Next-to-Next-to-Leading*, *Phys. Rev. Lett.* **97** (2006) 122002, [hep-ph/0605203].
- [109] G. Isidori and R. Unterdorfer, *On the short distance constraints from $K_{L,S} \rightarrow \mu^+\mu^-$* , *JHEP* **01** (2004) 009, [hep-ph/0311084].
- [110] G. Ecker and A. Pich, *The Longitudinal muon polarization in $K_L \rightarrow \mu^+\mu^-$* , *Nucl. Phys. B* **366** (1991) 189–205.
- [111] G. D’Ambrosio and T. Kitahara, *Direct CP Violation in $K \rightarrow \mu^+\mu^-$* , *Phys. Rev. Lett.* **119** (2017), no. 20 201802, [arXiv:1707.06999].
- [112] A. Dery, M. Ghosh, Y. Grossman, and S. Schacht, *$K \rightarrow \mu^+\mu^-$ as a clean probe of short-distance physics*, *JHEP* **07** (2021) 103, [arXiv:2104.06427].
- [113] A. J. Buras, F. Schwab, and S. Uhlig, *Waiting for precise measurements of $K^+ \rightarrow \pi^+\nu\bar{\nu}$ and $K_L \rightarrow \pi^0\nu\bar{\nu}$* , *Rev. Mod. Phys.* **80** (2008) 965–1007, [hep-ph/0405132].
- [114] F. Mescia and C. Smith, *Improved estimates of rare K decay matrix-elements from $K_{\ell 3}$ decays*, *Phys. Rev. D* **76** (2007) 034017, [arXiv:0705.2025].
- [115] V. Cirigliano, G. Ecker, H. Neufeld, A. Pich, and J. Portoles, *Kaon Decays in the Standard Model*, *Rev. Mod. Phys.* **84** (2012) 399, [arXiv:1107.6001].
- [116] A. J. Buras, M. Gorbahn, U. Haisch, and U. Nierste, *Charm quark contribution to $K^+ \rightarrow \pi^+\nu\bar{\nu}$ at next-to-next-to-leading order*, *JHEP* **11** (2006) 002, [hep-ph/0603079]. [Erratum: JHEP 11, 167 (2012)].
- [117] J. Brod and M. Gorbahn, *Electroweak Corrections to the Charm Quark Contribution to*

- $K^+ \rightarrow \pi^+ \nu \bar{\nu}$, *Phys. Rev. D* **78** (2008) 034006, [arXiv:0805.4119].
- [118] G. Isidori, F. Mescia, and C. Smith, *Light-quark loops in $K \rightarrow \pi \nu \bar{\nu}$* , *Nucl. Phys. B* **718** (2005) 319–338, [hep-ph/0503107].
- [119] L. S. Littenberg, *The CP Violating Decay $K_L^0 \rightarrow \pi^0 \nu \bar{\nu}$* , *Phys. Rev. D* **39** (1989) 3322–3324.
- [120] G. Buchalla and G. Isidori, *The CP conserving contribution to $K_L \rightarrow \pi^0 \nu \bar{\nu}$ in the standard model*, *Phys. Lett. B* **440** (1998) 170–178, [hep-ph/9806501].
- [121] G. Buchalla and A. J. Buras, *$K_L \rightarrow \pi \nu \bar{\nu}$ and high precision determinations of the CKM matrix*, *Phys. Rev. D* **54** (1996) 6782–6789, [hep-ph/9607447].
- [122] W. J. Marciano and Z. Parsa, *Rare kaon decays with “missing energy”*, *Phys. Rev. D* **53** (1996), no. 1 R1.
- [123] S. L. Glashow, J. Iliopoulos, and L. Maiani, *Weak Interactions with Lepton-Hadron Symmetry*, *Phys. Rev. D* **2** (1970) 1285–1292.
- [124] G. Eilam, J. L. Hewett, and A. Soni, *Rare decays of the top quark in the standard and two Higgs doublet models*, *Phys. Rev. D* **44** (1991) 1473–1484. [Erratum: *Phys. Rev. D* **59**, 039901 (1999)].
- [125] J. A. Aguilar-Saavedra, *Top flavor-changing neutral interactions: Theoretical expectations and experimental detection*, *Acta Phys. Polon. B* **35** (2004) 2695–2710, [hep-ph/0409342].
- [126] J. J. Zhang, C. S. Li, J. Gao, H. X. Zhu, C. P. Yuan, and T.-C. Yuan, *Next-to-leading order QCD corrections to the top quark decay via the Flavor-Changing Neutral-Current operators with mixing effects*, *Phys. Rev. D* **82** (2010) 073005, [arXiv:1004.0898].
- [127] J. Drobnak, S. Fajfer, and J. F. Kamenik, *Flavor Changing Neutral Coupling Mediated Radiative Top Quark Decays at Next-to-Leading Order in QCD*, *Phys. Rev. Lett.* **104** (2010) 252001, [arXiv:1004.0620].
- [128] J. Drobnak, S. Fajfer, and J. F. Kamenik, *QCD Corrections to Flavor Changing Neutral Coupling Mediated Rare Top Quark Decays*, *Phys. Rev. D* **82** (2010) 073016, [arXiv:1007.2551].
- [129] M. Jezabek and J. H. Kuhn, *QCD Corrections to Semileptonic Decays of Heavy Quarks*, *Nucl. Phys. B* **314** (1989) 1–6.
- [130] A. Czarnecki, *QCD corrections to the decay $t \rightarrow Wb$ in dimensional regularization*, *Phys. Lett. B* **252** (1990) 467–470.
- [131] C. S. Li, R. J. Oakes, and T. C. Yuan, *QCD corrections to $t \rightarrow W^+b$* , *Phys. Rev.* **D43** (1991) 3759–3762.

- [132] **Particle Data Group** Collaboration, P. Zyla et al., *Review of Particle Physics*, *PTEP* **2020** (2020), no. 8 083C01.
- [133] **Fermilab Lattice, MILC, TUMQCD** Collaboration, A. Bazavov et al., *Up-, down-, strange-, charm-, and bottom-quark masses from four-flavor lattice QCD*, *Phys. Rev. D* **98** (2018), no. 5 054517, [arXiv:1802.04248].
- [134] **CKMfitter Group** Collaboration, J. Charles, A. Hocker, H. Lacker, S. Laplace, F. R. Le Diberder, J. Malcles, J. Ocariz, M. Pivk, and L. Roos, *CP violation and the CKM matrix: Assessing the impact of the asymmetric B factories*, *Eur. Phys. J. C* **41** (2005), no. 1 1–131, [hep-ph/0406184]. Updated results and plots available at: <http://ckmfitter.in2p3.fr>.
- [135] **HFLAV** Collaboration, Y. S. Amhis et al., *Averages of b-hadron, c-hadron, and τ -lepton properties as of 2018*, *Eur. Phys. J. C* **81** (2021) 226, [arXiv:1909.12524]. updated results and plots available at <https://hflav.web.cern.ch/>.
- [136] **ALEPH** Collaboration, R. Barate et al., *Measurements of $\mathcal{B}(b \rightarrow \tau^- \bar{\nu}_\tau X)$ and $\mathcal{B}(b \rightarrow \tau^- \bar{\nu}_\tau D^{*\pm} X)$ and upper limits on $\mathcal{B}(B^- \rightarrow \tau^- \bar{\nu}_\tau)$ and $\mathcal{B}(b \rightarrow s \nu \bar{\nu})$* , *Eur. Phys. J. C* **19** (2001) 213–227, [hep-ex/0010022].
- [137] **Belle** Collaboration, J. Grygier et al., *Search for $B \rightarrow h \nu \bar{\nu}$ decays with semileptonic tagging at Belle*, *Phys. Rev. D* **96** (2017), no. 9 091101, [arXiv:1702.03224]. [Addendum: Phys.Rev.D 97, 099902 (2018)].
- [138] **LHCb** Collaboration, R. Aaij et al., *Constraints on the $K_S^0 \rightarrow \mu^+ \mu^-$ Branching Fraction*, *Phys. Rev. Lett.* **125** (2020), no. 23 231801, [arXiv:2001.10354].
- [139] **NA62** Collaboration, E. Cortina Gil et al., *Measurement of the very rare $K^+ \rightarrow \pi^+ \nu \bar{\nu}$ decay*, arXiv:2103.15389.
- [140] **KOTO** Collaboration, J. K. Ahn et al., *Search for the $K_L \rightarrow \pi^0 \nu \bar{\nu}$ and $K_L \rightarrow \pi^0 X^0$ decays at the J-PARC KOTO experiment*, *Phys. Rev. Lett.* **122** (2019), no. 2 021802, [arXiv:1810.09655].
- [141] **ATLAS** Collaboration, ATLAS, *Search for flavor-changing neutral-current couplings between the top quark and the Z boson with LHC Run2 proton-proton collisions at $\sqrt{s} = 13$ TeV with the ATLAS detector*, .
- [142] D. M. Straub, *flavio: a Python package for flavour and precision phenomenology in the Standard Model and beyond*, arXiv:1810.08132.
- [143] W. Altmannshofer, C. Niehoff, P. Stangl, and D. M. Straub, *Status of the $B \rightarrow K^* \mu^+ \mu^-$ anomaly after Moriond 2017*, *Eur. Phys. J. C* **77** (2017), no. 6 377, [arXiv:1703.09189].

- [144] W. Altmannshofer, P. Stangl, and D. M. Straub, *Interpreting Hints for Lepton Flavor Universality Violation*, *Phys. Rev. D* **96** (2017), no. 5 055008, [arXiv:1704.05435].
- [145] J. Aebischer, W. Altmannshofer, D. Guadagnoli, M. Reboud, P. Stangl, and D. M. Straub, *B-decay discrepancies after Moriond 2019*, *Eur. Phys. J. C* **80** (2020), no. 3 252, [arXiv:1903.10434].
- [146] **LHCb** Collaboration, R. Aaij et al., *Differential branching fractions and isospin asymmetries of $B \rightarrow K^{(*)}\mu^+\mu^-$ decays*, *JHEP* **06** (2014) 133, [arXiv:1403.8044].
- [147] **CDF** Collaboration, CDF, *Precise Measurements of Exclusive $b \rightarrow s\mu^+\mu^-$ Decay Amplitudes Using the Full CDF Data Set*, .
- [148] **CMS** Collaboration, V. Khachatryan et al., *Angular analysis of the decay $B^0 \rightarrow K^{*0}\mu^+\mu^-$ from pp collisions at $\sqrt{s} = 8$ TeV*, *Phys. Lett. B* **753** (2016) 424–448, [arXiv:1507.08126].
- [149] **LHCb** Collaboration, R. Aaij et al., *Measurements of the S-wave fraction in $B^0 \rightarrow K^+\pi^-\mu^+\mu^-$ decays and the $B^0 \rightarrow K^*(892)^0\mu^+\mu^-$ differential branching fraction*, *JHEP* **11** (2016) 047, [arXiv:1606.04731]. [Erratum: JHEP 04, 142 (2017)].
- [150] **LHCb** Collaboration, R. Aaij et al., *Differential branching fraction and angular analysis of $\Lambda_b^0 \rightarrow \Lambda\mu^+\mu^-$ decays*, *JHEP* **06** (2015) 115, [arXiv:1503.07138]. [Erratum: JHEP 09, 145 (2018)].
- [151] **BaBar** Collaboration, J. P. Lees et al., *Measurement of the $B \rightarrow X_s l^+ l^-$ branching fraction and search for direct CP violation from a sum of exclusive final states*, *Phys. Rev. Lett.* **112** (2014) 211802, [arXiv:1312.5364].
- [152] **LHCb** Collaboration, R. Aaij et al., *Angular analysis of charged and neutral $B \rightarrow K\mu^+\mu^-$ decays*, *JHEP* **05** (2014) 082, [arXiv:1403.8045].
- [153] **Belle** Collaboration, S. Wehle et al., *Lepton-Flavor-Dependent Angular Analysis of $B \rightarrow K^* l^+ l^-$* , *Phys. Rev. Lett.* **118** (2017), no. 11 111801, [arXiv:1612.05014].
- [154] **CMS** Collaboration, CMS, *Measurement of the P_1 and P'_5 angular parameters of the decay $B^0 \rightarrow K^{*0}\mu^+\mu^-$ in proton-proton collisions at $\sqrt{s} = 8$ TeV*, .
- [155] **ATLAS** Collaboration, M. Aaboud et al., *Angular analysis of $B_d^0 \rightarrow K^*\mu^+\mu^-$ decays in pp collisions at $\sqrt{s} = 8$ TeV with the ATLAS detector*, *JHEP* **10** (2018) 047, [arXiv:1805.04000].
- [156] **LHCb** Collaboration, R. Aaij et al., *Angular analysis of the rare decay $B_s^0 \rightarrow \phi\mu^+\mu^-$* , arXiv:2107.13428.
- [157] **LHCb** Collaboration, R. Aaij et al., *Angular moments of the decay $\Lambda_b^0 \rightarrow \Lambda\mu^+\mu^-$ at low hadronic recoil*, *JHEP* **09** (2018) 146, [arXiv:1808.00264].

- [158] B. Capdevila, A. Crivellin, S. Descotes-Genon, J. Matias, and J. Virto, *Patterns of New Physics in $b \rightarrow s\ell^+\ell^-$ transitions in the light of recent data*, *JHEP* **01** (2018) 093, [[arXiv:1704.05340](#)].
- [159] A. K. Alok, A. Dighe, S. Gangal, and D. Kumar, *Continuing search for new physics in $b \rightarrow s\mu\mu$ decays: two operators at a time*, *JHEP* **06** (2019) 089, [[arXiv:1903.09617](#)].
- [160] M. Algueró, B. Capdevila, S. Descotes-Genon, J. Matias, and M. Novoa-Brunet, *$b \rightarrow s\ell\ell$ global fits after Moriond 2021 results*, in *55th Rencontres de Moriond on QCD and High Energy Interactions*, 4, 2021. [arXiv:2104.08921](#).
- [161] T. Hurth, F. Mahmoudi, D. M. Santos, and S. Neshatpour, *More Indications for Lepton Nonuniversality in $b \rightarrow s\ell^+\ell^-$* , [arXiv:2104.10058](#).
- [162] W.-S. Hou, M. Kohda, and T. Modak, *Search for tZ' associated production induced by tcZ' couplings at the LHC*, *Phys. Rev. D* **96** (2017), no. 1 015037, [[arXiv:1702.07275](#)].
- [163] S. Cho, P. Ko, J. Lee, Y. Omura, and C. Yu, *Top FCNC induced by a Z' boson*, *Phys. Rev. D* **101** (2020), no. 5 055015, [[arXiv:1910.05925](#)].
- [164] E. Alvarez, A. Juste, M. Szewc, and T. Vazquez Schroeder, *Topping-up multilepton plus b -jets anomalies at the LHC with a Z' boson*, *JHEP* **05** (2021) 125, [[arXiv:2011.06514](#)].
- [165] **CMS Collaboration**, A. M. Sirunyan et al., *Search for associated production of a Z boson with a single top quark and for tZ flavour-changing interactions in pp collisions at $\sqrt{s} = 8$ TeV*, *JHEP* **07** (2017) 003, [[arXiv:1702.01404](#)].
- [166] **CMS Collaboration** Collaboration, C. Collaboration, *Search for flavour changing neutral currents in top quark production and decays with three-lepton final state using the data collected at $\sqrt{s} = 13$ TeV*, Tech. Rep. CMS-PAS-TOP-17-017, CERN, Geneva, 2017.
- [167] **ATLAS Collaboration**, M. Aaboud et al., *Search for flavour-changing neutral current top-quark decays $t \rightarrow qZ$ in proton-proton collisions at $\sqrt{s} = 13$ TeV with the ATLAS detector*, *JHEP* **07** (2018) 176, [[arXiv:1803.09923](#)].
- [168] G. Durieux, F. Maltoni, and C. Zhang, *Global approach to top-quark flavor-changing interactions*, *Phys. Rev. D* **91** (2015), no. 7 074017, [[arXiv:1412.7166](#)].
- [169] M. Chala, J. Santiago, and M. Spannowsky, *Constraining four-fermion operators using rare top decays*, *JHEP* **04** (2019) 014, [[arXiv:1809.09624](#)].
- [170] J. Gao, C. S. Li, and H. X. Zhu, *Top Quark Decay at Next-to-Next-to Leading Order in QCD*, *Phys. Rev. Lett.* **110** (2013), no. 4 042001, [[arXiv:1210.2808](#)].
- [171] **ATLAS Collaboration**, A. Collaboration, *Sensitivity of searches for the flavour-changing neutral current decay $t \rightarrow qZ$ using the upgraded ATLAS experiment at*

the High Luminosity LHC, .

- [172] Y.-B. Liu and S. Moretti, *Probing tqZ anomalous couplings in the trilepton signal at the HL-LHC, HE-LHC and FCC-hh*, [arXiv:2010.05148](#).
- [173] S. Behera, R. Islam, M. Kumar, P. Poulose, and R. Rahaman, *Fingerprinting the Top quark FCNC via anomalous Ztq couplings at the LHeC*, *Phys. Rev.* **D100** (2019), no. 1 015006, [[arXiv:1811.04681](#)].
- [174] S. Khatibi and M. Moallemi, *Probing FCNC couplings in single top quark production associated with a neutral gauge boson at future lepton colliders*, [arXiv:2106.08231](#).
- [175] Y. Afik, S. Bar-Shalom, A. Soni, and J. Wudka, *New flavor physics in di- and trilepton events from single-top production at the LHC and beyond*, *Phys. Rev. D* **103** (2021), no. 7 075031, [[arXiv:2101.05286](#)].
- [176] **Belle-II** Collaboration, W. Altmannshofer et al., *The Belle II Physics Book*, *PTEP* **2019** (2019), no. 12 123C01, [[arXiv:1808.10567](#)]. [Erratum: *PTEP* 2020, 029201 (2020)].